blood®
Regular Article

LYMPHOID NEOPLASIA

The proto-oncogene TCL1A deregulates cell cycle and genomic stability in CLL

Johanna Stachelscheid,[1-3] Qu Jiang,[1-3] Christoph Aszyk,[1-3] Kathrin Warner,[1,4] Nadine Bley,[5] Tony Müller,[1-3] Olga Vydzhak,[1-3] Konstantinos Symeonidis,[1-3] Giuliano Crispatzu,[1-3] Petra Mayer,[1-3] Stuart James Blakemore,[1-3] Gudrun Goehring,[6] Sebastian Newrzela,[4] Stephanie Hippler,[1] Sandra Robrecht,[1] Karl-Anton Kreuzer,[1] Christian Pallasch,[1-3] Marcus Krüger,[2,3] Axel Lechner,[7] Kirsten Fischer,[1] Stephan Stilgenbauer,[8,9] Dirk Beutner,[7] Michael Hallek,[1-3] Daniel Auguin,[10,11] Stefan Hüttelmaier,[5] Johannes Bloehdorn,[8,*] Elena Vasyutina,[1-3,*] and Marco Herling[1-3,12,*]

[1]Department I of Internal Medicine, Center for Integrated Oncology Aachen Bonn Cologne Duesseldorf (CIO ABCD), University Hospital Cologne, Cologne, Germany; [2]Center for Molecular Medicine Cologne (CMMC) and [3]Cologne Excellence Cluster on Stress Responses in Aging-Associated Diseases (CECAD), University of Cologne, Cologne, Germany; [4]Senckenberg Institute of Pathology, Goethe-University, Frankfurt am Main, Germany; [5]Section for Molecular Cell Biology, Institute of Molecular Medicine, Faculty of Medicine, Martin Luther University Halle-Wittenberg, Charles Tanford Protein Center, Halle, Germany; [6]Institute of Human Genetics, Hannover Medical School, Hannover, Germany; [7]Department of Otorhinolaryngology, University of Göttingen, Göttingen, Germany; [8]Department of Internal Medicine III, Ulm University, Ulm, Germany; [9]Department of Internal Medicine I, Saarland University Medical Center, Homburg, Germany; [10]Université d'Orléans, INRA, USC1328, Orléans, France; [11]Structural Motility, Institut Curie, Paris Université Sciences et Lettres, Sorbonne Université, CNRS, Paris, France; and [12]Department of Hematology, Cellular Therapy, and Hemostaseology, University of Leipzig, Leipzig, Germany

KEY POINTS

- **TCL1A directly engages CDC20 in the mitotic checkpoint complex, accelerating cell cycle transit and driving genome instability in B cells.**
- **Downregulated CDC20 in CLL cells resembles the aneuploidy phenotype and is associated with more aggressive disease and cellular features.**

Upregulation of the proto-oncogene T-cell leukemia/lymphoma 1A (*TCL1A*) is causally implicated in various B-cell and T-cell malignancies. High-level TCL1A correlates with aggressive disease features and inferior clinical outcomes. However, the molecular and cell biological consequences of, particularly nuclear, TCL1A are not fully elucidated. We observed here in mouse models of subcellular site-specific TCL1A-induced lymphomagenesis that TCL1A exerts a strong transforming impact via nuclear topography. In proteomic screens of TCL1A-bound molecules in chronic lymphocytic leukemia (CLL) cells and B-cell lymphoma lines, we identified regulators of cell cycle and DNA repair pathways as novel TCL1A interactors, particularly enriched under induced DNA damage and mitosis. By functional mapping and in silico modeling, we specifically identified the mitotic checkpoint protein, cell division cycle 20 (CDC20), as a direct TCL1A interactor. According to the regulatory impact of TCL1A on the activity of the CDC20-containing mitotic checkpoint and anaphase-promoting complexes during mitotic progression, TCL1A overexpression accelerated cell cycle transition in B-cell lymphoma lines, impaired apoptotic damage responses in association with pronounced chromosome missegregation, and caused cellular aneuploidy in *Eμ-TCL1A* mice. Among hematopoietic cancers, *CDC20* levels seem particularly low in CLL. *CDC20* expression negatively correlated with *TCL1A* and lower expression marked more aggressive and genomically instable disease and cellular phenotypes. Knockdown of Cdc20 in TCL1A-initiated murine CLL promoted aneuploidy and leukemic acceleration. Taken together, we discovered a novel cell cycle–associated effect of TCL1A abrogating controlled cell cycle transition. This adds to our concept of oncogenic TCL1A by targeting genome stability. Overall, we propose that TCL1A acts as a pleiotropic adapter molecule with a synergistic net effect of multiple hijacked pathways.

Introduction

T-cell leukemia/lymphoma 1A (*TCL1A*) is the prototypic member of a 3-paralogue family that further includes *TCL1B* and mature T-cell proliferation 1 (*MTCP1*). Upregulation of TCL1A owing to rearrangements of its gene locus on chromosome 14 is considered the initiating event in T-prolymphocytic leukemia (T-PLL).[1,2] Deregulated TCL1A is also implicated in the pathogenesis of chronic lymphocytic leukemia (CLL).[3]

Both T-PLL and CLL show elevated TCL1A expression in >90% of cases, yet at variable levels. Highest levels are associated with more complex karyotypes, high-risk (cyto)genetic aberrations, unfavorable clinical features, such as faster tumor cell doubling,[2,4-6] and poorer responses to chemoimmunotherapies.[4-7] Analogous observations were made in other B-cell lymphomas.[8-10]

The transforming capacity of TCL1A in T and B cells has been demonstrated in transgenic (tg) mouse models. Animals

expressing human *TCL1A* under the murine T-cell specific *Lck* promoter or the B-cell receptor *VH* promoter/*IGHμ* enhancer develop expansions that closely resemble human T-PLL (*Lck*^{pr}-*TCL1A* mice)[11] or CLL (*Eμ-TCL1A* mice),[12] respectively.

The 14 kDa beta barrel–shaped TCL1A protein lacks enzymatic properties and does not possess DNA-binding activity. Its best established oncogenic function is an adapter-like engagement of induced homodimers in subplasmalemmal molecular complexes with AKT, leading to nuclear translocalization and catalytic augmentation of this oncogenic serine/threonine kinase.[13,14] TCL1A can also enhance NF-κB and inhibit AP-1 transcriptional activities.[15] We characterized TCL1A as a threshold-lowering sensitizer toward antigen receptor signals, mainly mediated by an activating physical interaction with involved cytoplasmic kinases.[5,6,16] As constitutively active myristoylated (myr) AKT in murine B cells does not recapitulate the oncogenic effect of TCL1A,[17] we postulate an underrecognized target pleiotropism of TCL1A.[18] In particular, the molecular effectors of nuclear TCL1A are not well established.

We also observed a cell cycle–dependent protein expression of TCL1A at the single-cell level in CLL and other B-cell tumors.[4,9] This implicates TCL1A as an intricate component of deregulated cell cycle pathways, which are central to B-cell leukemogenesis.[19-21]

Generally, the checkpoints that regulate cell cycle progression after DNA replication are the G2/M checkpoint, which ensures DNA integrity before prophase entry, and the mitotic checkpoint (also known as spindle assembly checkpoint), which prevents premature cell division until all kinetochores are attached to a spindle.[22,23] The mitotic checkpoint is maintained by the mitotic checkpoint complex (MCC), which antagonizes the multisubunit anaphase-promoting complex (APC/C), an E3 ubiquitin-ligase mediating the onset of the anaphase. The cell division cycle 20 (CDC20) plays a crucial role in both complexes. By acting as a coactivator of the APC/C (APC/C^{CDC20}), it promotes anaphase initiation.[23] As part of the MCC, however, it also inhibits the function of APC/C^{CDC20} together with mitotic arrest deficient 2 (MAD2) and the mitotic checkpoint proteins, BUBR1 and BUB3.[24]

Here, we demonstrate that TCL1A perturbs cell cycle transition and impedes an adequate DNA damage response (DDR), resulting in genome instability. We implicate protein interactions of TCL1A with components of the MCC and APC/C, such as CDC20, to mediate these effects. Associations with aggressive disease characteristics and clinical outcomes emphasize a central role of (deregulated) CDC20 in CLL.

Materials and methods

Patient material

Peripheral blood (PB)–derived healthy donor (Institutional Blood Bank) and CLL samples (Departmental Biorepository) were obtained under institutional review board–approved protocols (#11-319, #01-143, #9-1085, and #13-091) with written informed consent according to the Declaration of Helsinki. Ficoll-isolated PB mononuclear cells and B cells were purified and cultured as reported.[25]

Mouse experiments

Studies on *Eμ-TCL1A* mice[12] were carried out under permission 84-02.04.2012.A394 (Regional Council, Cologne, Germany). Preleukemic stage: white blood cell (WBC) counts <25 × 10^9/L (age, 7-8 weeks) and no hepatosplenomegaly; and overt leukemic stage: >30% CD5$^+$/19$^+$ population in PB and a WBC count >50 × 10^9/L.

For primary murine hematopoietic stem cell and progenitor cell (HSC/HPC) transplantations (F21/03 and FK/1050, Regional Council, Darmstadt, Germany), bone marrow cells were isolated from B6-SJL mice, and lineage-committed cells were depleted as described.[26] Remaining cells were retrovirally transduced with vectors MP91-eGFP, human (h)TCL1A, myr-hTCL1A, or nuclear localization signal (nls)-hTCL1A. After irradiation, 1 × 10^6 transduced cells were transplanted into C57BL/6 recipients.

IPs, MS, and validations

Immunoprecipitations (IPs) with specific antibodies were carried out using the following beads: streptavidin-coupled (biotinylated proteins; Sigma-Aldrich, St. Louis, MO), Anti-FLAG M2 magnetic beads (FLAG-tagged proteins, Sigma), Ni2$^+$ resins (his-tagged proteins, Sigma), and Protein G Sepharose (Sigma) or magnetic Dynabeads Protein G (Invitrogen, Waltham, MA). Eluates and input samples were analyzed by immunoblots. Samples and mass spectrometry (MS) protocols, as well as details on the proximity ligation assay (PLA) and the protein complementation assay are provided in the supplemental Data, available on the *Blood* website.

Cell cycle analysis

Cells were synchronized via nocodazole (Sigma) at 100 ng/mL for 16 hours or with RO-3306 (Selleckchem, Houston, TX) at 9 μM for 20 hours. Cells were washed, released into full medium, and harvested at indicated time points. Cellular DNA content was measured by Hoechst 33258 (Sigma) staining in the presence of RNase A (Invitrogen) using the IntraPrep Permeabilization kit (Beckman Coulter, Brea, CA). Analysis on the Gallios flow cytometer used the Kaluza software (both Beckman Coulter).

Profiling experiments

Array-based gene expression profiles (GEPs) were performed on tumor cell suspensions (>70% B-cell content) from spleens of recipients of HSC/HPC, transduced with site-targeted TCL1A versions or with enhanced green fluorescent protein (eGFP) (CD19$^+$GFP$^+$ cells at day 100). Gene set enrichment analysis (GSEA) used the GSEA_4.0.3 software (Broad Institute, Cambridge, MA). Microarray GEP of 337 human CLL8 trial samples and data analyses are outlined in the supplemental Data and in Hallek et al.,[27] Vasyutina et al.,[28] and Bloehdorn et al.[29] For single-cell RNA sequencing of splenocytes of *Eμ-TCL1A* mice see Kohlhaas et al.[30] and supplemental Data.

Results

TCL1A exerts a strong oncogenic impact via its nuclear localization

TCL1A is expressed in the cytoplasm and in the nucleus of CLL cells (supplemental Figure 1A). To refine the concept of subcellular site-specific leukemogenic effects of TCL1A, we transduced murine HSC/HPC with 3 human *TCL1A* variants:

wild-type (WT), membrane-targeted myr-TCL1A, and nuclear-localized nls-TCL1A (Figure 1A). Localization of these TCL1A forms was validated in HEK293T cells and in situ (spleens of induced lymphomas) (Figure 1B; supplemental Figure 1B). Mice transplanted with cells expressing nls-hTCL1A had a significantly shorter lymphoma-specific survival than mice with WT-TCL1A–induced tumors (median, 349 days vs 388 days, respectively; Figure 1C), despite similar disease characteristics and histologies (supplemental Figure 1C). All 3 groups developed mostly B-cell leukemias/lymphomas and less frequently CD4/CD8 double-positive/negative T-cell leukemias/lymphomas (supplemental Table 1). GSEA of GEP data from the B-cell tumors identified nuclear pathways including DNA repair, cell cycle, and mitotic spindle to be enriched in the nls-hTCL1A vs WT-TCL1A–induced lymphomas (Figure 1D-E; supplemental Table 2). These pathways were also enriched in all TCL1A conditions compared with GFP control B cells (supplemental Figure 2). We concluded a preferential B-cell oncogenic function of TCL1A in the nuclear compartment, especially in the context of DNA repair and cell cycle regulation.

TCL1A is part of protein complexes that regulate DDR and cell cycle

To characterize TCL1A's interactome in a more unbiased fashion, MS analyses of TCL1A-IPs were performed in human CLL samples (N = 11 [supplemental Table 3]; divided into IGHV-unmutated CLL (U-CLL) and IGHV-mutated CLL (M-CLL) [Figure 2A] or into 3 cytogenetic/clinical-risk categories [supplemental Figure 3]) and in tonsillar B cells (N = 3). In total, 889 and 459 TCL1A-interacting proteins were identified in tonsillar B cells and CLL cells, respectively (groups vs IgG control; fold change (FCh) >2, FDR q < 0.05; supplemental

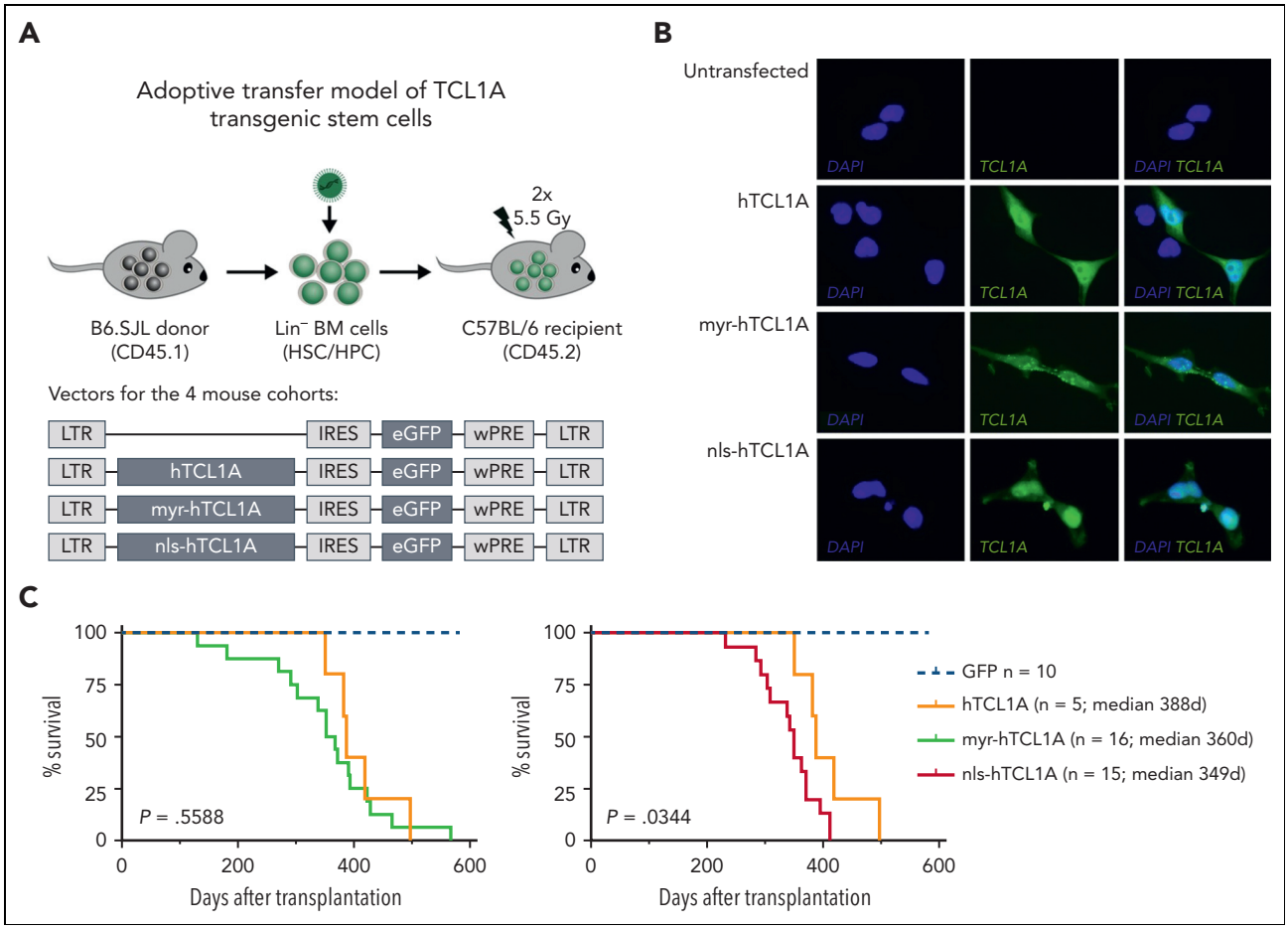

Figure 1. Pronounced oncogenic function of nuclear TCL1A. (A) Experimental setup of adoptive transfer of hTCL1A transgenic stem cells, HSC/HPC isolated from B6.SJL donor mice, were retrovirally transduced with vectors expressing different variants of hTCL1A (bottom). hTCL1A: unrestricted WT TCL1A; myr-hTCL1A: membrane-targeted TCL1A expression; nls-hTCL1A: nuclear enrichment of TCL1A. After transduction, cells were injected into bone marrow–depleted C57BL/6 mice. (B) Immunofluorescence images of HEK293T cells retrovirally transduced with 3 different TCL1A variants, validating their subcellular localization. Images were captured at original magnification ×60 using an Axio Scope.A1 fluorescent microscope (Zeiss, Germany). For subcellular distribution of TCL1A in the lymphomatous spleens, see supplemental Figure 1B. (C) Kaplan-Meier curves of mice transplanted with HSC/HPC, expressing generic hTCL1A (orange, N = 5), myr-hTCL1A (green, N = 16), and nls-hTCL1A (red, N = 15). Log-rank test showed a significantly shorter survival of nls-hTCL1A than the hTCL1A-recipient mice. For an overview of disease characteristics of transplanted mice, see supplemental Table 1, and for histology of organs, see supplemental Figure 1C. (D) Gene expression of splenocytes from mice with B-cell malignancies (>70% tumor cell content) was analyzed via microarrays. GSEA identified several deregulated pathways between lymphomas of nls-hTCL1A- vs hTCL1A-recipient mice (false discovery rate [FDR] <0.05). Identified nuclear pathways are upregulated in tumor cells from nls-hTCL1A recipients. Deregulated pathways for TCL1A variants vs GFP only and myr-hTCL1a vs nls-TCL1A are displayed in supplemental Figure 2. (E) Enrichment plots of significantly deregulated pathways involved in cell cycle and in DNA repair between nls-hTCL1A- and hTCL1A-expressing cells. IFNγ, interferon γ; IL2, interleukin 2; IRES, internal ribosomal entry site; LTR, long terminal repeat; TNFα, tumor necrosis factor α; wPRE, woodchuck hepatitis virus post-transcriptional regulatory element.

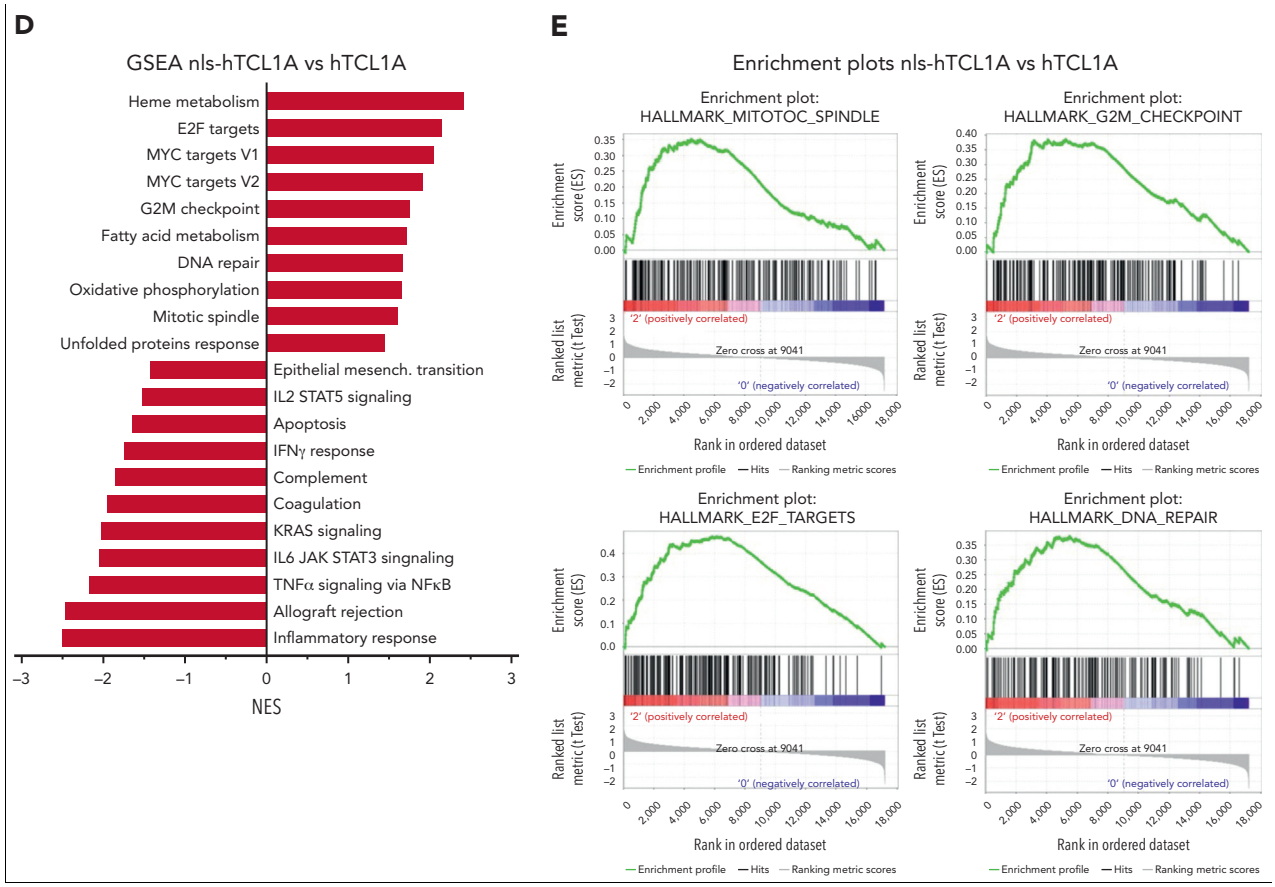

Figure 1 (continued)

Table 4). The interactome of TCL1A was independent of disease subset, as most interacting partners overlapped across the genetic and clinical categories (Figure 2B; supplemental Figure 3B). ORA identified a variety of pathways within the TCL1A interactome in CLL, suggesting a pleiotropic perturbation of cellular processes by TCL1A. Among them, several nuclear pathways were identified, including 'cell cycle' as the third largest functional network cluster identified in the TCL1A interactome, further emphasizing the relevance of nuclear TCL1A (Figure 2C-D; supplemental Figure 4; supplemental Table 5). It included important proteins regulating cell cycle transition, such as the protein kinase ATM (G2/M checkpoint, DNA repair),[32] MCM proteins (DNA replication checkpoint),[33] and NEK9 (mitotic checkpoint)[34] (Figure 2E-F). These findings suggest an important role of TCL1A in the regulation of the DDR and cell cycle transition.

TCL1A interacts with proteins of the MCC

This novel pronunciation of nuclear effectors of TCL1A prompted us to analyze the interactome of TCL1A after specific activation signals, that is, genotoxic stress and mitosis induction, in the B-PLL–derived cell line JVM3 (hardly expresses TCL1A). Stable overexpression of TCL1A (JVM3^{TCL1A}) conferred a phenotype of resistance to the classical DNA-targeting chemotherapeutics: doxorubicin, cyclophosphamide, and etoposide (supplemental Figure 5). MS analysis of TCL1A pull-downs from JVM3^{TCL1A} vs JVM3^{GFP} cells that were left untreated, exposed to DNA damage induction (etoposide), or synchronized in enforced mitosis (nocodazole) identified a total of 962 TCL1A-interacting proteins (FCh >2, FDR q < 0.05; Figure 3A-B; supplemental Tables 6 and 7), with a marked increase after genotoxic or mitotic stimulation (a total of 76 interactors in the untreated condition vs 245 under genotoxic stress vs 736 in enforced mitosis) (Figure 3B). Most TCL1A-interacting proteins were exclusively detected in mitosis (N = 674), whereas 164 proteins specifically bound to TCL1A under genotoxic stress.

The functional pathway clusters within these TCL1A interactomes identified by ORA were highly dependent on the condition (Figure 3C-D; supplemental Tables 8-10). Under genotoxic stress and mitosis, cell cycle and cell cycle checkpoints were highly prominent recurrent pathways, with cell cycle being the second biggest cluster in the TCL1A interactome of JVM3 cells synchronized in mitosis (Figure 3C). Importantly, proteins involved in the regulation of the APC/C, as components of the MCC (eg, CDC20 and MAD2) or subunits of the APC/C (eg, CDC27), were specifically present in the mitotic condition, suggesting a function of TCL1A in the composition and regulation of the mitotic checkpoint (Figure 3E). We confirmed the interaction of TCL1A with CDC20, MAD2, and CDK1 in B cells of *Eμ-TCL1A* mice and in human CLL cells via co-IP (Figure 4A-B).

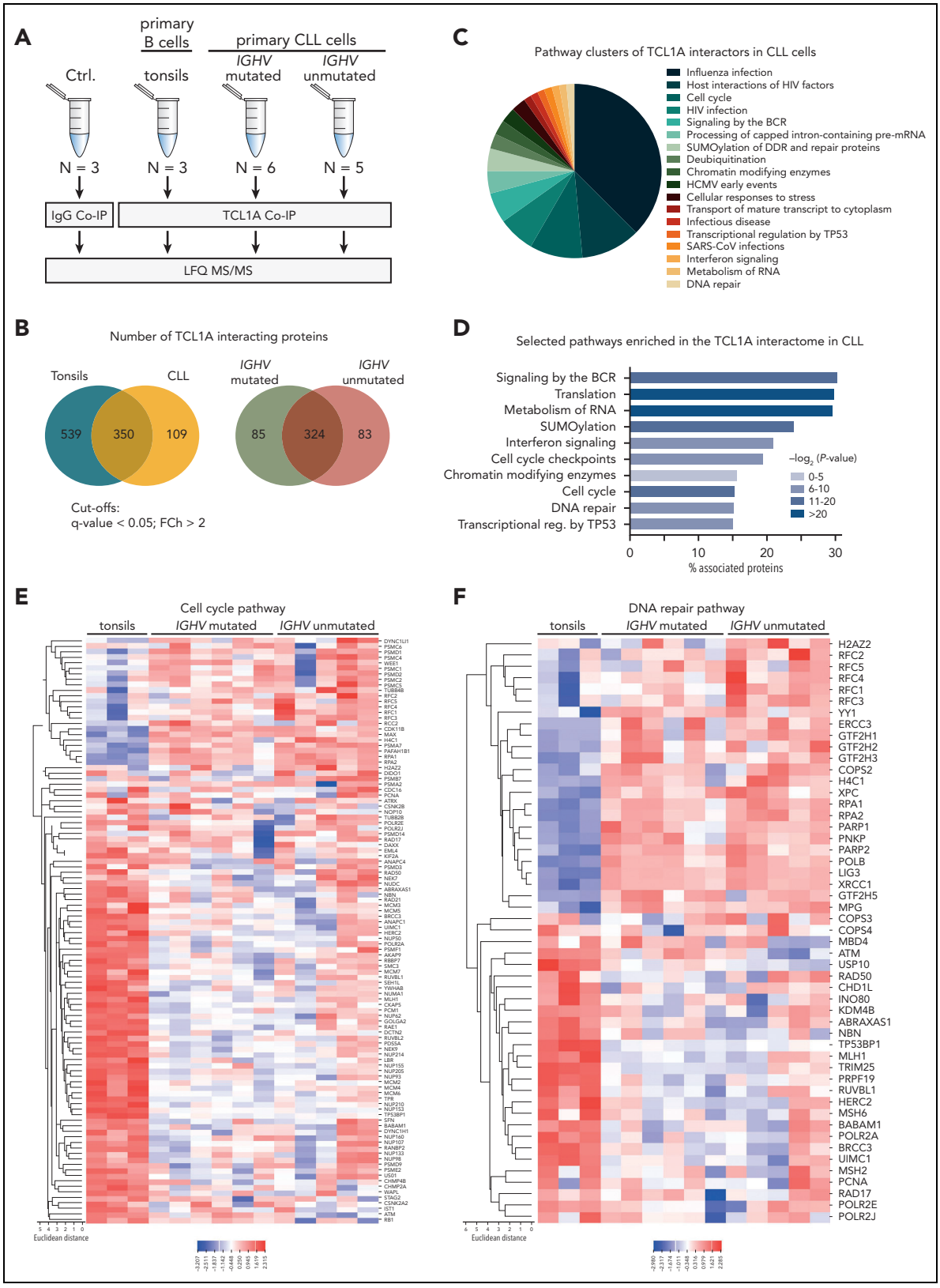

Figure 2. Proteins involved in the DNA repair and the cell cycle pathways are common interaction partners of TCL1A. (A) Experimental setup: TCL1A coimmunoprecipitations (co-IPs) were performed from lysates of primary CLL cells, divided into 2 subgroups based on their IGHV gene mutation status. Primary B cells isolated from tonsils were used as healthy controls (N = 3). Co-IPs with immunoglobulin G (IgG) served as a negative control (N = 3, CLL lysates). Processed immunoprecipitates were analyzed on a label-free quantification (LFQ) LC-MS/MS device. (B) Venn diagrams showing the overlap of identified TCL1A-interacting proteins between healthy B cells from tonsils and CLL cells, as well as between U-CLL and M-CLL (for the comparison of cytogenetic/clinical-risk groups "no go" vs "slow go" vs "high-risk," see supplemental Figure 3). Proteins were considered interactors when they were significantly enriched in the corresponding group vs IgG control (FDR $q < 0.05$, FCh >2, Welsh test).

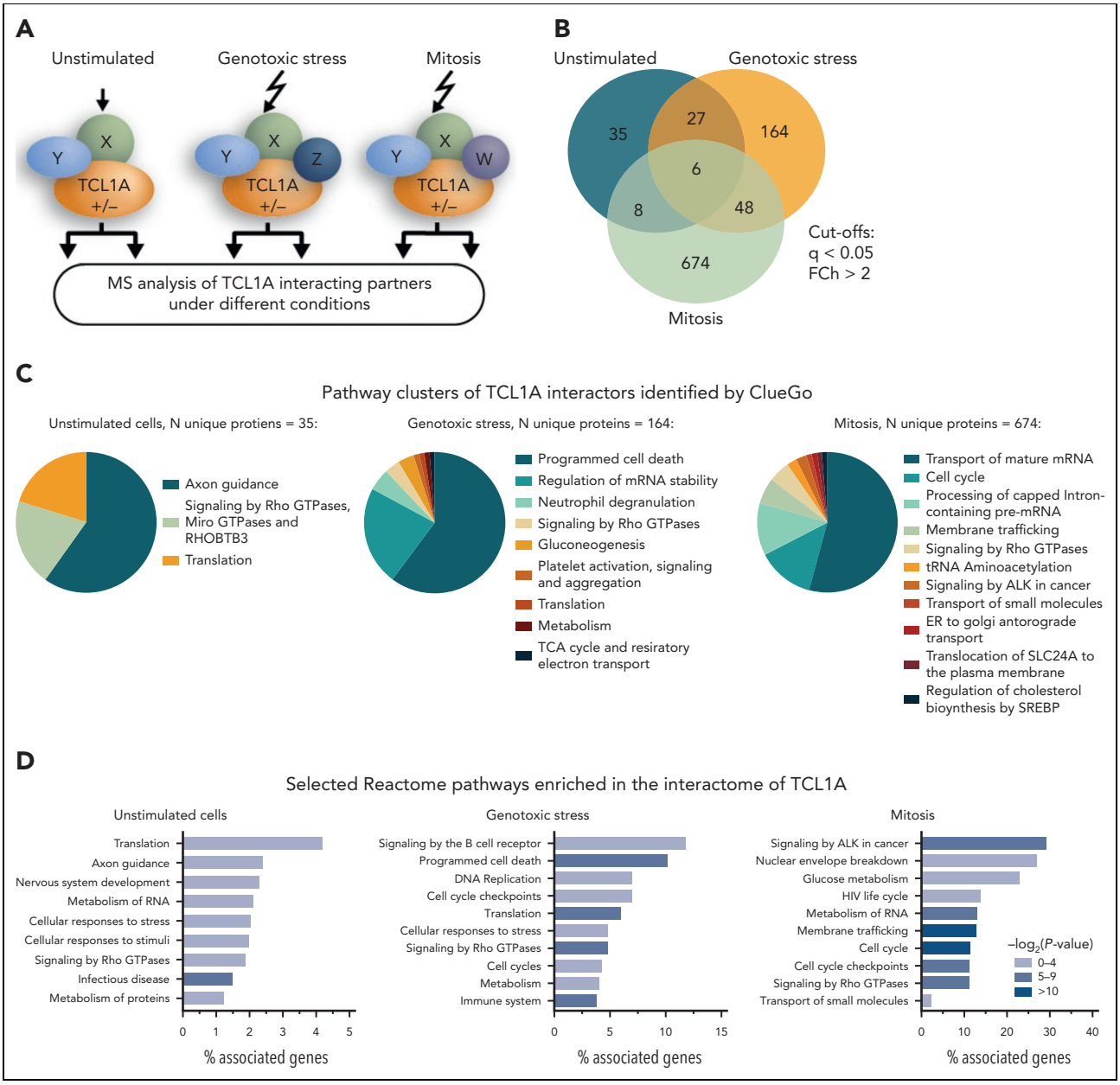

Figure 3. Systematic MS-based analysis of TCL1A interacting partners identifies mitotic checkpoint regulators. (A) Experimental setup: TCL1A-bound protein complexes were isolated from JVM3 CLL-like cells ± transfected TCL1A; at baseline (untreated culture), under genotoxic stress (5 μM etoposide for 4.5 hours) or synchronized in mitosis (100 ng/mL nocodazole for 18 hours, release for 1 hour), followed by LFQ LC-MS/MS MS. (B) MS identified in total 962 significantly TCL1A-interacting proteins (cutoffs per group: FDR $q < 0.05$, FCh >2; Student t test). Most proteins differentially interact with TCL1A in JVM3^{TCL1A} B cells only at baseline (blue), under genotoxic stress (yellow), or during mitosis (green). (C) Overview of enriched pathway clusters within the TCL1A interactome identified by ORA using Cytoscape plug-in ClueGO (version 2.5.8). Enriched pathways highly depend on the condition. (D) Overview of selected enriched pathways (Reactome pathway database) within the TCL1A interactome identified in panel C. (E) STRING network of TCL1A interactors involved in the cell cycle checkpoint of JVM3 cells under genotoxic stress (left) and synchronized in mitosis (right) identified by ClueGO. Colors indicate the involvement in the particular cell cycle checkpoint (green indicated G1/S transition; blue, G2/M checkpoint; red, separation of sister chromatids; yellow, inhibition of APC/C via direct inhibition of the APC/C complex). Note the marked network expansion upon mitosis induction. Mitotic checkpoint proteins (eg, CDC20, MAD2, and CDC27, a subunit of the APC/C E3 ubiquitin-ligase complex) appear centrally involved in TCL1A signaling in mitosis only. ER, endoplasmic reticulum; TCA, trichloroacetic acid; tRNA, transfer RNA.

Figure 2 (continued) (C) Overview of enriched pathway clusters within the TCL1A interactome identified by overrepresentation analysis (ORA) using the Cytoscape plug-in ClueGO (version 2.5.8, Reactome database), indicating the percentage of terms per cluster. Supplemental Figure 4 shows the associated functional networks of all enriched pathways identified by ClueGO. (D) Bar graph of selected pathways identified in panel C illustrating the percentage of associated proteins from the TCL1A interactome within each pathway. Heat map of TCL1A interactors belonging to the cell cycle pathway (E) and the DNA repair pathway (F) as identified by ORA using ClueGO. BCR, B-cell receptor; HCMV, human cytomegalovirus; mRNA, messenger RNA; SARS-CoV, severe acute respiratory syndrome coronavirus.

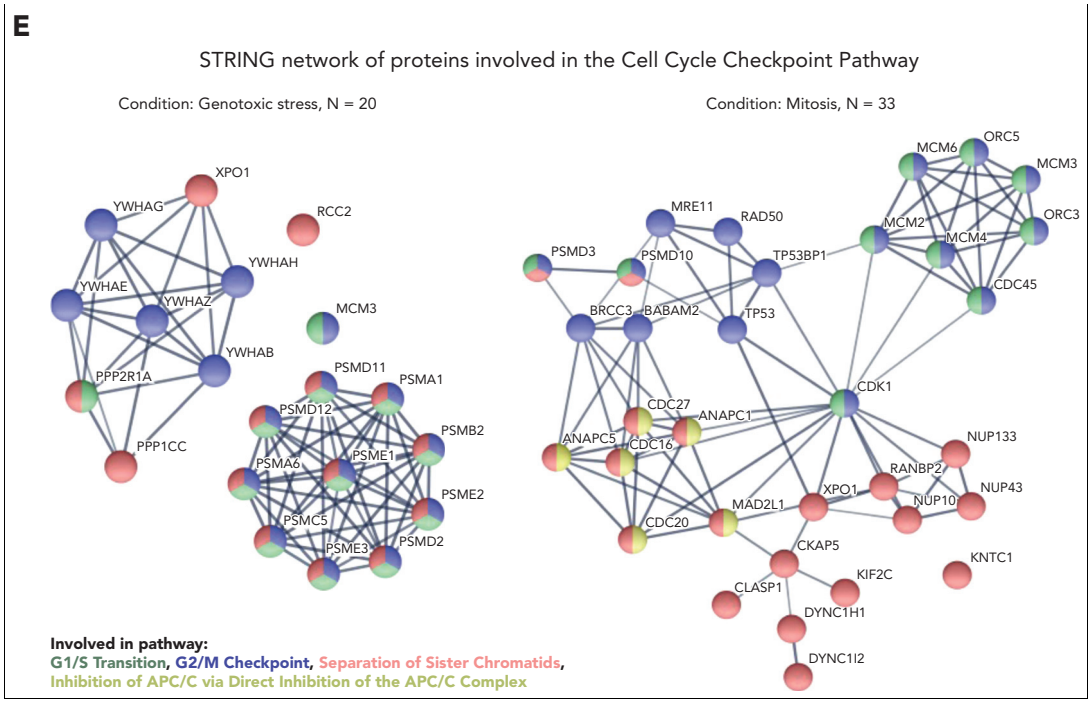

Figure 3 (continued)

TCL1A accelerates cell cycle transition of mitotic B cells

Investigating the impact of TCL1A on mitotic progression, we observed that the TCL1A-positive variants of JVM3, DoHH2, MEC1, and HEK293T cells had transitioned faster through mitosis already 3 to 5 hours after release from G2 synchronization as compared with TCL1A-negative controls (Figure 4C-E; supplemental Figure 6A). Protein levels of the APC/C targets, cyclin A and CDC20, degraded faster in TCL1A-positive cells. Furthermore, phosphorylation of central regulators of the G2/M checkpoint, including CDK1, that decline along the course of mitosis,[22,35] showed lower levels after release in TCL1A-positive cells (Figure 4E; supplemental Figure 6B). Phosphorylation of Aurora A/B/C, all involved in the mitotic checkpoint, was not markedly altered by TCL1A overexpression (supplemental Figure 6C-D).

To specifically dissect the effect of TCL1A on mitotic transit, we performed in vivo BrdU S phase–labeling experiments in leukemic *Eμ-TCL1A* vs WT mice. Splenocytes were isolated 20 hours after BrdU injection and stained for incorporated BrdU and pH3, as a marker for active mitosis. *Eμ-TCL1A* splenocytes showed significantly increased proliferation over WT splenocytes, indicated by a higher number of $BrdU^+$ ($P = .009$) and $pH3^+$ ($P = .012$) cells. A larger proportion of *Eμ-TCL1A* cells had exited mitosis within 20 hours after injection ($BrdU^+/pH3^-$ cells, $P = .01$). There were also significantly more $BrdU^-/pH3^+$ cells ($P = .01$) in the *Eμ-TCL1A* group after the BrdU pulse (Figure 4F). According to these data, TCL1A-positive B cells enter and exit the cell cycle more frequently, suggesting abnormal cell cycle passaging.

Aberrant DDR and aneuploidy in TCL1A-driven leukemia

We next investigated the impact of aberrant TCL1A expression on central regulators of the DDR, that is, ATM and p53. In primary CLL cells, high TCL1A levels (by quantitative reverse transcription polymerase chain reaction) correlated with reduced levels of phosphoactivated and cleaved ATM upon genotoxic stress (Figure 5A-B). Furthermore, B cells from *Eμ-TCL1A* mice show reduced p53 levels accompanied by an accumulation of TUNEL-positive double-strand breaks as compared with B cells from age-matched WT mice (Figure 5C).

Considering the observed protein interactions of TCL1A with MCC components, we investigated whether TCL1A negatively affects mitotic spindle formation and segregation, leading to increased chromosomal aberrations. Indeed, TCL1A-positive JVM3 and DoHH2 cells showed a higher frequency of multipolar spindles than their TCL1A-negative controls ($P = .032$ and $P = .029$, respectively), which was corroborated by shRNA-mediated TCL1A knockdown in MEC1 cells ($P = .041$) (Figure 5D). Moreover, we identified a higher number of polyploid cells in the $DoHH2^{TCL1A}$ and $JVM3^{TCL1A}$ lines compared with EV controls ($P = .006$ and $P = .005$, respectively; Figure 5E), alongside a trend to more complex karyotypes (Figure 5F).

In line with these findings, chromosomal aberrations were frequently detected in B cells from *Eμ-TCL1A* mice (Figure 5G), with aneuploidy already present at the preleukemic phase ($P = .03$) and even more pronounced at the overt leukemic stage ($P < .0001$; Figure 5H). These data implicate overexpressed TCL1A to perturb genomic integrity via impaired DDRs and aberrant spindle formation (chromatid segregation).

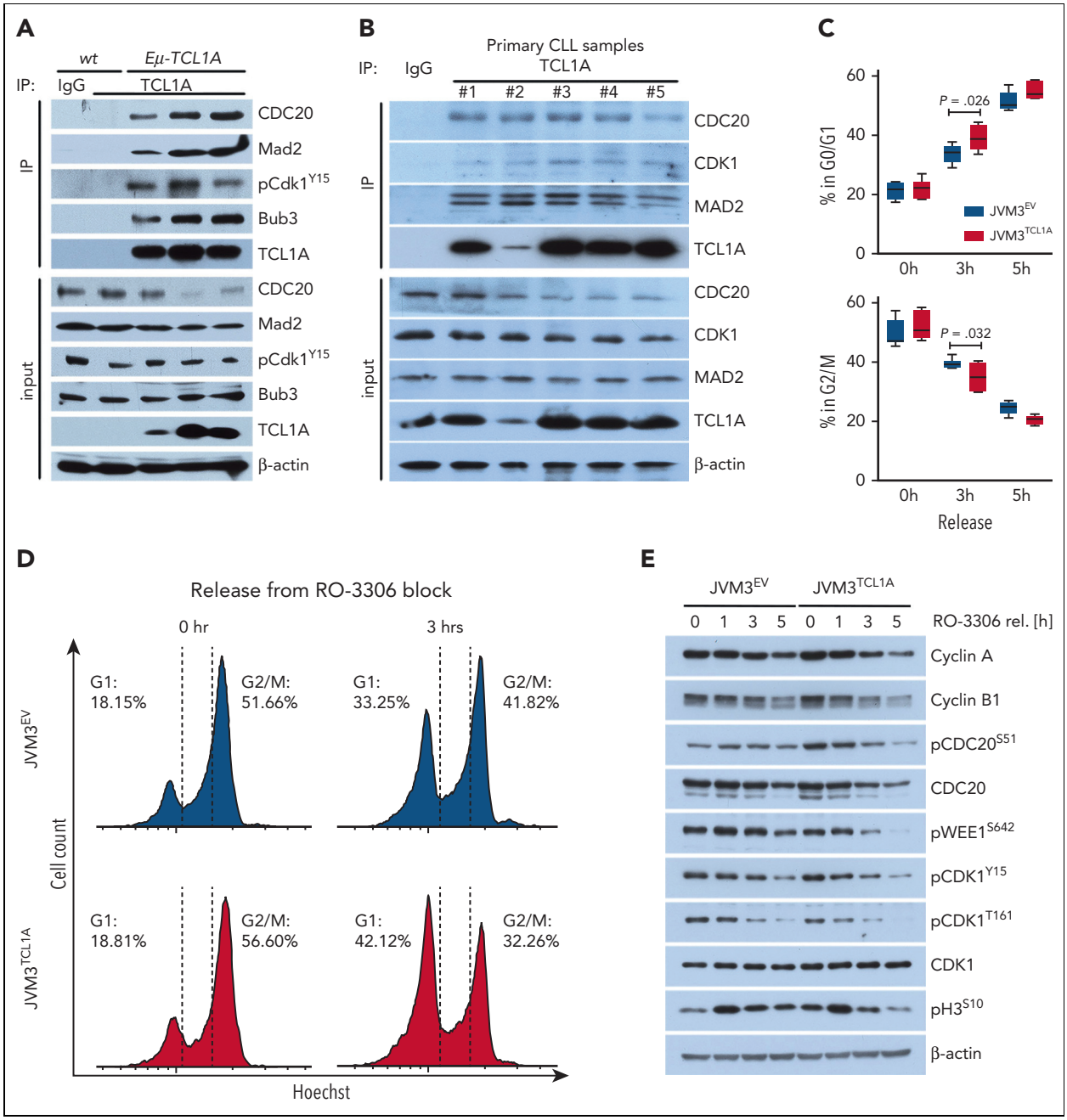

Figure 4. TCL1A overexpression leads to aberrant cell cycle progression. (A) Immunoblots of co-IPs of B cells from spleens of WT or *Eμ-TCL1A* mice using anti-TCL1A antibodies or isotype IgG (negative control). Lanes represent individual animals. (B) Immunoblots of co-IPs using IgG controls or specific TCL1A antibodies in primary CLL samples cocultured with differentiated THP-1 monocytic cells in the presence of CpG and IL-15 for 36 hours to induce proliferation. Lanes represent individual CLL samples. (C) Box plot showing percentages of cells in G0/G1 (top) and G2/M (bottom) of JVM3 ± TCL1A that were released from RO-3306 synchronization from 4 independent experiments. Boxes display medians with 25th to 75th percentiles and whiskers of 5th to 95th percentiles. Significances were estimated by the Mann-Whitney test. Analogous results for HEK293T and DoHH2 cells (TCL1A introduction) as well as for MEC1 cells (short hairpin RNA (shRNA)–mediated TCL1A knockdown) are shown in supplemental Figure 6A. (D) Flow-cytometric analysis of G2/M synchronized (via RO-3306 for 20 hours) JVM3 cells ± TCL1A stained with Hoechst. Representative histogram shows an accelerated exit from the G2/M into the G1 cell cycle phase after release in full medium of TCL1A-overexpressing cells. The blue area indicates JVM3 empty vector (EV) and red area indicates JVM3^{TCL1A}. (E) Representative immunoblot from lysates of cells released from RO-3306–mediated synchronization. JVM3^{TCL1A} cells show faster dephosphorylation of proteins involved in the regulation of cell cycle transition as well as a faster degradation of cyclin A and B and CDC20. Analogous results for HEK293T and DoHH2 cells (TCL1A introduction) as well as for MEC1 cells (TCL1A knockdown) are shown in supplemental Figure 6B. (F) Aberrant cell cycle progression in TCL1A-driven murine leukemia. *Eμ-TCL1A* mice (N = 4) or age-matched WT controls (N = 3) were injected with 5-bromo-2′-deoxyuridine (BrdU) (top). At 20 hours after injection, the ratios of BrdU$^+$ (in S phase at time of injection, green), phosphorylated histone 3$^+$ (pH3$^+$) (in mitosis at time of harvest, red), BrdU$^+$;pH3$^+$ (formerly in S phase, currently mitotic, yellow), and BrdU$^-$;pH3$^-$ (not proliferating, blue) cell counts were determined by immunostaining (2500 cells per animal; Student *t* test). Images were captured at original magnification ×60 using an Axio Scope.A1 fluorescent microscope. Increased overall proliferation (S phase and mitosis) of *Eμ-TCL1A* cells (BrdU$^+$ and pH3$^+$) (bottom). These *TCL1A*-transgenic cells exited the cell cycle more often (higher proportion of BrdU$^+$;pH3$^-$ and similar proportion of BrdU$^+$/pH3$^+$ cells). An increased population of BrdU$^-$/pH3$^+$ cells in the *Eμ-TCL1A* cohort also suggests that they re-enter the cell cycle more frequently.

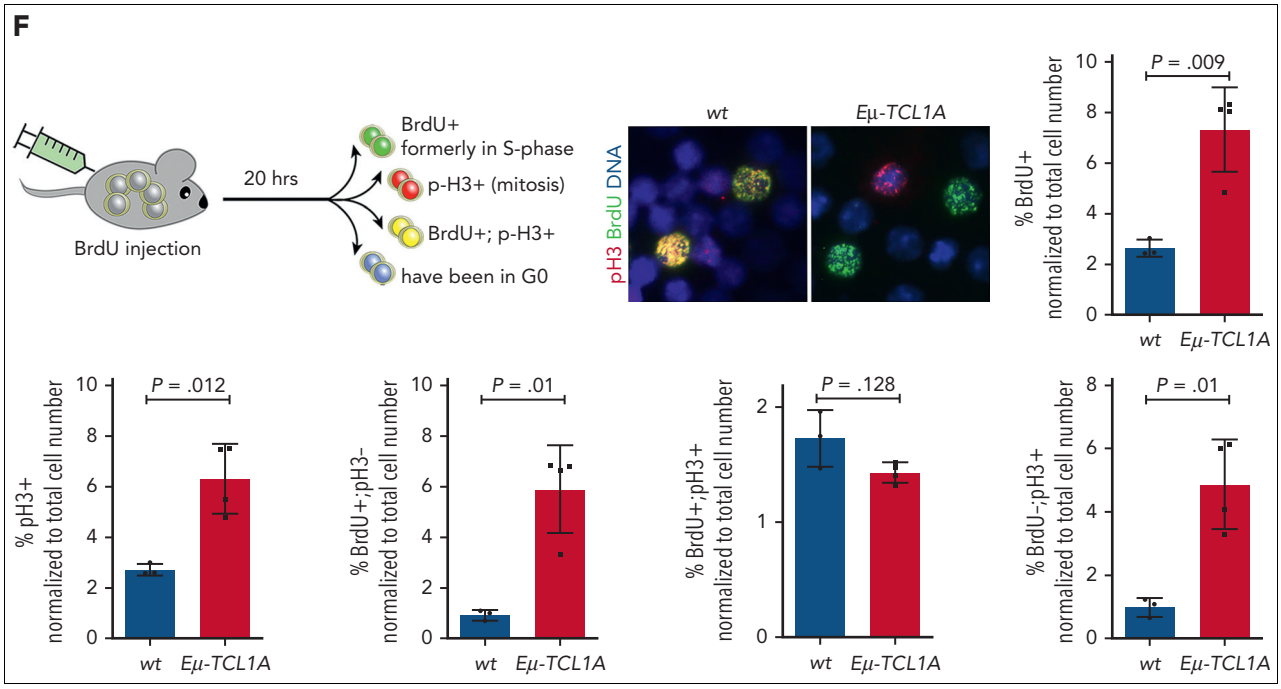

Figure 4 (continued)

TCL1A and CDC20 directly interact during mitosis

To assess the involvement of TCL1A in the MCC, we investigated the interaction of TCL1A with selected targets. PLAs identified interactions of TCL1A with CDC20, MAD2, and the G2/M checkpoint protein CDK1 in the cytoplasm as well as along the spindles of MEC1 cells (Figure 6A; supplemental Figure 7A-B). The TCL1A-CDC20 interaction increased from interphase to prophase and persisted during mitosis (Figure 6B; supplemental Figure 7C-D).

As CDC20 is one of the key proteins controlling mitotic checkpoint transition, we validated the interaction of TCL1A with CDC20 by split-reporter protein complementation assay,[38] which facilitate intracellular detection of direct protein-protein interactions based on complementation of N/C-terminal YFP components (Figure 6C). Immunofluorescence microscopy of HeLa cells harboring TCL1A-YFP^{N} and CDC20-YFP^{C} constructs demonstrated a direct TCL1A-CDC20 interaction, which accumulated at the mitotic plate and dispersed during anaphase (Figure 6D). Homodimerization of TCL1A was not a prerequisite for this interaction, as WT TCL1A and the dimerization-defective mutant PLT^{3A} equally bound to CDC20 (supplemental Figure 7E).

Defined sites in CDC20 are involved in the interaction with TCL1A

CDC20 activity is controlled by several regulatory sequences such as the KEN- and CRY-boxes, which are targets of phosphorylation and which engage APC/C substrates.[23,39,40] The C-boxes facilitate interaction with the APC/C,[40] whereas the MIM is required for the interaction with MAD2. To identify functional motifs of CDC20 involved in the interaction with TCL1A, we generated 5 CDC20 mutants: (1) del97-169 lacking KEN-, MIM-, and CRY-box; (2) RCRY^{4A}: R132>A and CRY165-167>AAA (inactivating MIM- and CRY-box); (3) R^{A}: R132>A (inactivating MIM-box); (4) CRY^{3A}: CRY165-167>AAA (inactivating CRY-box); (5) KEN^{3A}: KEN97-99>AAA (inactivating KEN-box) (Figure 6E). The mutations in the KEN, CRY, and MIM motifs are described as not altering the protein structure of CDC20.[41]

Expression vectors encoding TCL1A were cotransfected into HEK293 cells alongside one of the CDC20 mutants or CDC20^{WT} constructs. Subsequent co-IPs revealed that mutations in the KEN sequence (KEN^{3A}) did not affect the CDC20-TCL1A interaction. Mutations in the CRY-box (CRY^{3A}) led to a slightly reduced CDC20-TCL1A interaction. Interestingly, aa substitutions in the MIM sequence (R132A; R^{A}) resulted in a significantly impaired CDC20-TCL1A interaction. A simultaneous mutation of MIM and CRY sequences (RCRY^{4A}) or a deletion of the KEN, MIM, and CRY sequences (del97-169) almost completely abolished the interaction (Figure 6E).

In silico modeling resolves the CDC20-TCL1A complex structure

To refine and validate our model derived from this functional motif mapping, we performed a thorough in silico prediction of the CDC20-TCL1A complex based on published experimental protein structures of CDC20 (pdb ID 4GGA) and TCL1A (pdb ID 1JSG) using CPORT and HADDOCK 2.2.[37,42] CDC20 contains a central core of a 7-bladed β-propeller and 2 mobile extensions at the N and C termini.[43] Importantly, the 4 aa that were involved in the interaction with TCL1A (C165, R166, Y167, and R132) are located at the N terminus of CDC20, creating a joint interface. In accordance with the X-ray structure, the R166 side chain of the CRY-box rotates toward the core of CDC20 through

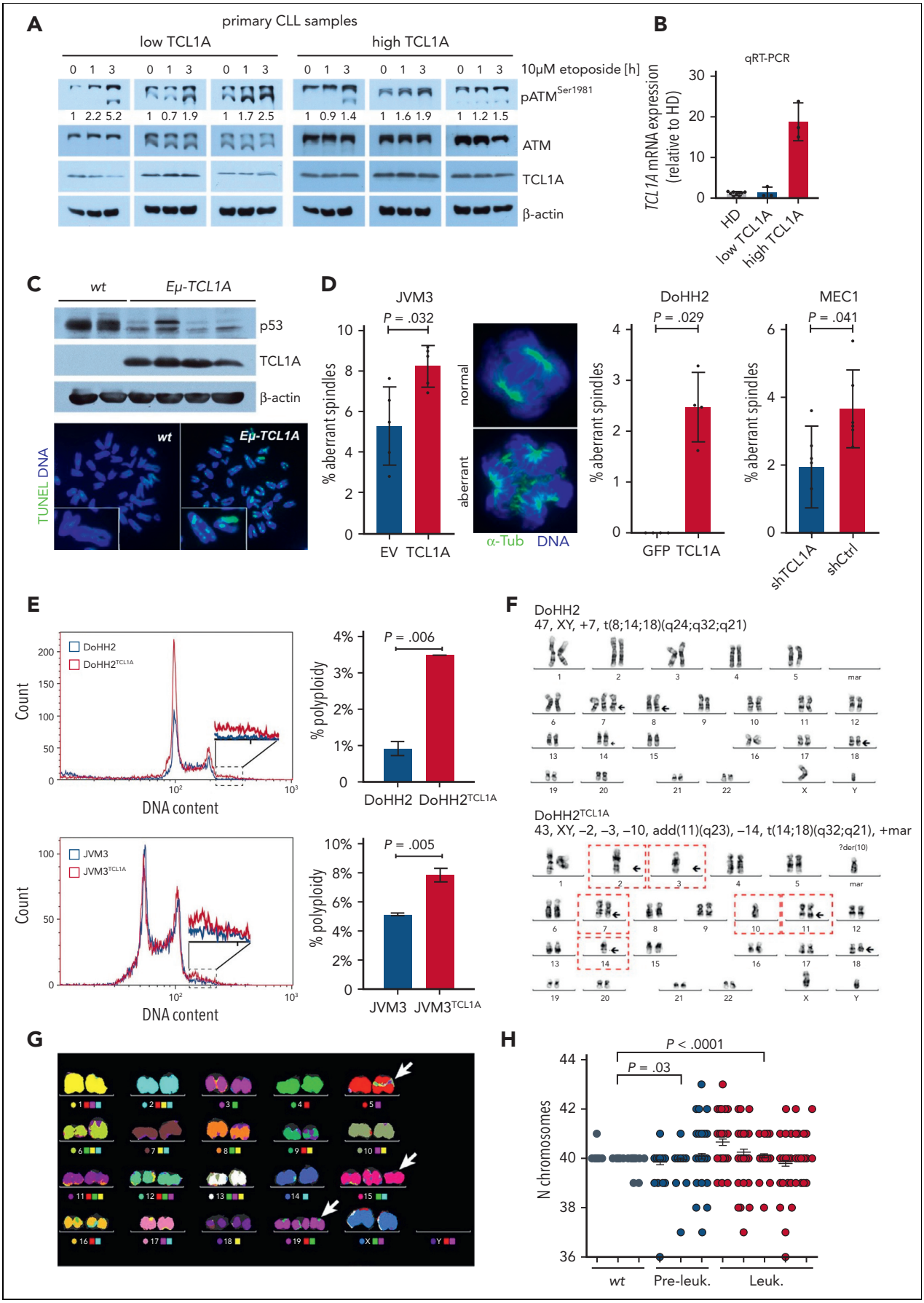

Figure 5.

a stable interaction with the negatively charged residue E413 (2.7 Å). This conformation of the CRY-box preserves a favorable docking interface for TCL1A. Substitution of R166 by alanine (CRY^{3A}) results in the loss of the stabilizing salt bridge, thereby weakening the TCL1A-CDC20 interaction (supplemental Figure 7F).

The HADDOCK 2.2 algorithm predicted 2 models that involve interactions of key aa of TCL1A (E9, E40, K42, R93, and Y96) which are prone to forming hydrogen bonds (or salt bridges) with respective residues of CDC20 (K440, E438, D173, and Y167; Figure 6F; supplemental Table 12). The predicted residues of TCL1A would get near the aa CRY165-167 of CDC20. The residues E40, K42, and Y96 of TCL1A are expected to stabilize the TCL1A-CDC20 interaction in model A, whereas E9, R93, and Y96 would promote this interaction in model B. For each model, HADDOCK statistics are displayed in supplemental Table 13. To validate these in silico models, we generated 2 TCL1A mutants fused to a FLAG-tag and stably overexpressed them in JVM3 cells: (1) EKY^{SAE}: E40S, K42A, Y96E (model A) and (2) ERY^{KDE}: E9K, R93D, Y96E (model B) (Figure 6G). The ERY^{KDE} aa substitutions did not affect the TCL1A-CDC20 interaction, whereas EKY^{SAE} nearly abolished it, supporting in silico model A. Overall, these in silico models together with the IP data on CDC20 and TCL1A mutants confirm and provide the structural basis for the direct TCL1A-CDC20 interaction. This, in turn, corroborates the concept of a modulatory impact of TCL1A on the activity of the MCC and/or APC/C during mitotic progression.

TCL1A impairs the interaction of CDC20 with MAD2 and PLK1

As MAD2 binding to CDC20 is crucial for a productive mitotic checkpoint,[44] we analyzed the influence of TCL1A on the CDC20-MAD2 interaction in mitotic MEC1 and HG3 cells (each ± TCL1A) via PLAs. There was a pronounced decrease in detected CDC20-MAD2 interactions in both TCL1A-high lines compared with the respective control cells (Figure 6H), which was validated in JVM3 cells via co-IPs (supplemental Figure 7G). Next to the sequestration of CDC20 by MAD2, its binding to the APC/C is negatively regulated via phosphorylation by PLK1.[45] In CDC20 co-IPs in JVM3 cells released from G2, we detected faster decreases of CDC20-PLK1 interactions already 1 hour after release when TCL1A was present (Figure 6I), suggesting a TCL1A-mediated impaired negative regulation of CDC20 by PLK1. Together, this defines a novel molecular mechanism on the modulatory impact of TCL1A on the proficiency of the mitotic checkpoint by impairing the interaction of CDC20 with its negative regulators.

Lower CDC20 expression correlates with features of aggressive CLL

Besides this novel interaction of TCL1A with CDC20, there have been no reports on CDC20 in CLL in general. *CDC20* was no target for mutations or copy number alterations in large CLL series (copy number alteration, N = 319 CLL;[29] mutations, N = 1308 CLL; cBioPortal).[46-49] We, therefore, analyzed its mRNA expression using publicly available gene expression databases[50] and identified a pronounced *CDC20* downregulation that was specific to CLL among several hematopoietic neoplasms (Figure 7A). At the protein level, we detected lower CDC20 in the more aggressive U-CLL than in M-CLL, which inversely correlated with TCL1A expression (Figure 7B).

This negative correlation was confirmed in GEP of patients included in the prospective CLL8 trial, which compared the outcome after fludarabine/cyclophosphamide treatment with or without rituximab (R) (FC vs FCR) (Figure 7C).[27] The expression of *CDC20* and *TCL1A* correlated with levels of key DDR and cell cycle–regulating genes, including *ATM* and *TP53* (supplemental Figure 8A-C). Significantly higher WBC counts were observed in the *CDC20*-low group (median, 101.3 vs 78.4 G/L for low vs high *CDC20* levels, respectively; $P = .003$; Figure 7D). Moreover, in univariate analyses, low *CDC20* expression was associated with shorter PFS of patients in the FC arm of the trial (median, 25.5 vs 34.1 months for low vs high *CDC20*, respectively; $P = .014$; Figure 7E; supplemental Table 14). As no effect on PFS was observed for patients in the FCR arm (supplemental Figure 8D), it is tempting to speculate that a CDC20 effect is overridden by the impact of the immunotherapeutic component rituximab, which targets much less cell cycle–dependent than classical chemotherapy (ie, FC).

Moreover, in CLL subgroups that we previously defined by their molecular profiles,[29] *CDC20* expression was significantly lower in those cases that carry a genome instability signature ($P < .001$; Figure 7F). Together, CDC20 shows a specific downregulation in CLL and lower levels mark a more aggressive genomically instable disease.

Figure 5. TCL1A overexpression interferes with a proficient DDR and confers aneuploidy. (A) Immunoblot analysis of phosphorylated (p)ATM^{S1981} in freshly isolated CLL cells treated with 10 μM etoposide for the indicated time points. Samples with low TCL1A expression (by quantitative reverse transcription polymerase chain reaction [qRT-PCR]) show higher etoposide-induced phosphorylation and cleavage of ATM. (B) qRT-PCR analysis of *TCL1A* expression of patient samples from panel A. (C) Splenocytes from leukemic (Leuk.) (10 months) *Eμ-TCL1A* mice showed a lower expression of p53 than age-matched WT mice (top). TUNEL analysis of splenocytes from WT and *Eμ-TCL1A* mice shows more DNA breaks in TCL1A-transgenic cells (bottom). Images at original magnification ×60 on an Axio Scope.A1 fluorescent microscope. (D) JVM3 (N = 5, representative photographs next to bar chart) and DoHH2 (N = 4) cells, both ± transgenic TCL1A, as well as MEC1 cells (N = 5; ± shRNA-mediated TCL1A knockdown) were synchronized in G2 via treatment with 9 μM RO-3306 for 20 hours. At 30 minutes and 1 hour after release, the percentage of aberrant spindles was determined by immunohistochemistry; α-tubulin (α-Tub) (green) and Hoechst (blue). The TCL1A-transgenic JVM3 and DoHH2 cells showed a more pronounced accumulation of multipolar spindles as compared with controls, which was reproduced in opposite direction in MEC1 cells after shRNA-mediated TCL1A knockdown. Range of 300 to 700 individual cells per condition; Student *t* test. Immunofluorescence images were captured at original magnification ×60 using an IX83 fluorescent microscope (Olympus, Japan). (E) Flow-cytometric quantification of Hoechst staining in DoHH2 ± TCL1A (top, N = 3 per genotype) and JVM3 ± TCL1A (bottom, N = 5 per genotype). In both cell lines, increased DNA ploidy was found in the TCL1A-positive condition as compared with the respective control line. (F) G-banding–based karyotype analysis of DoHH2 ± TCL1A B cells. Comparison of representative karyograms of DoHH2-TCL1A (N = 42) to DoHH2 parental cells (N = 21) with a trend toward an increased genetic complexity (chromosome gains, losses, deletions, and translocations) in the TCL1A-transfected cells. Percent of cells with genomic aberrations: DoHH2, 14.3%; $DoHH2^{TCL1A}$, 23.8%; $P = .516$, Fisher exact test, quantification not illustrated. (G) Spectral karyotyping analysis of *Eμ-TCL1A* leukemic B cells shows karyotypes with trisomies of chromosomes 15 and 19 and translocations of chromosome 5. (H) Splenocytes from preleukemic (Pre-leuk.) (N = 3, WBC $<30 \times 10^9$ cells/L) or leukemic (N = 5, WBC $>50 \times 10^9$ cells/L) *Eμ-TCL1A* mice showed an aberrant number of chromosomes compared with WT (N = 3) mice; Student *t* test.

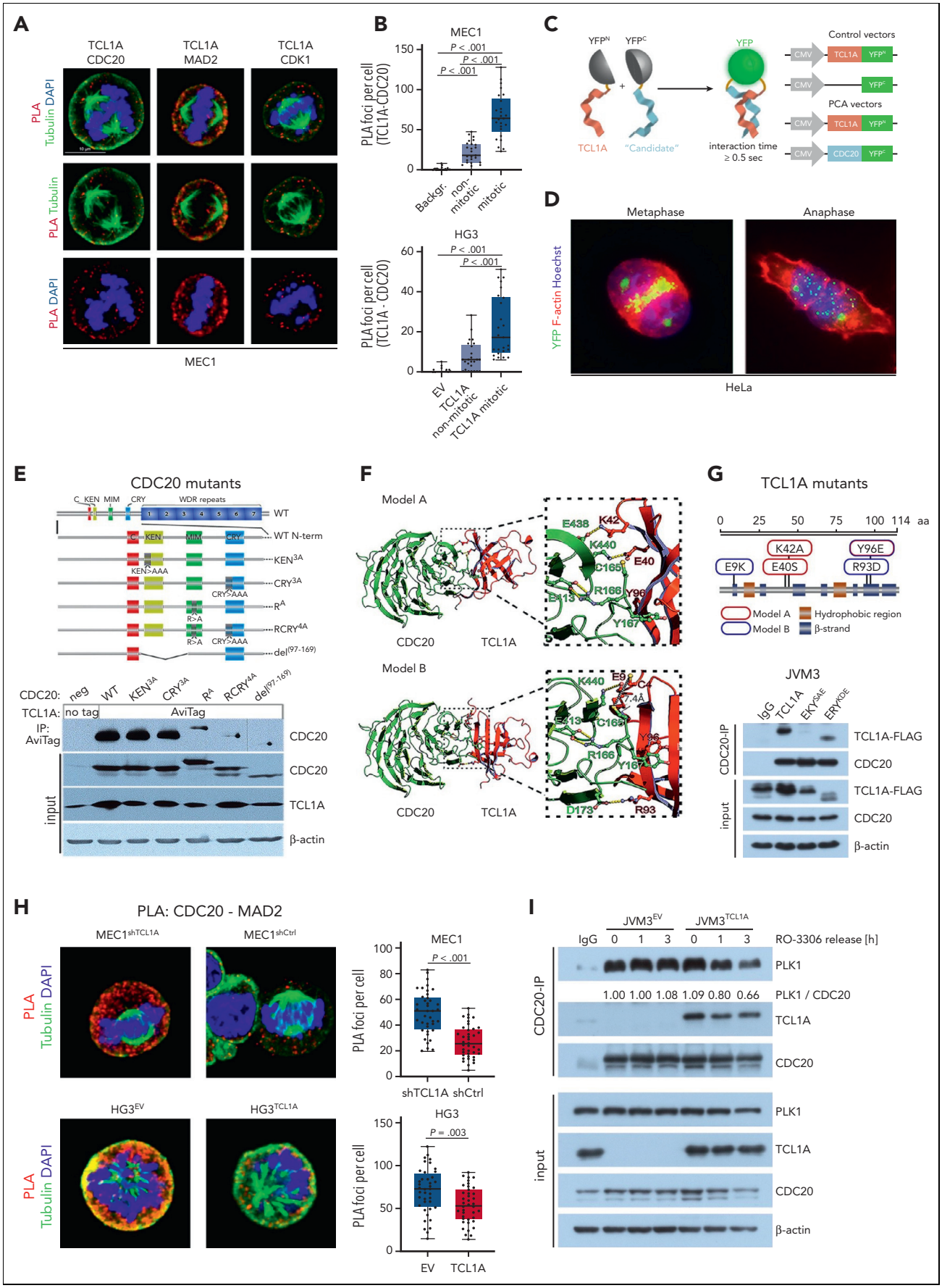

Figure 6.

Low CDC20 expression is a feature of aggressive *Eμ-TCL1A* cell populations

As in CLL samples, we also detected a reduced CDC20 protein expression in splenocytes of *Eμ-TCL1A* mice as compared with those from WT animals (supplemental Figure 9A). To assess the association of reduced *CDC20* expression with characteristics of cellular subsets, we made use of our previously published single-cell RNA sequencing data from *Eμ-TCL1A* mice and its derived allele *Eμ-TCL1A*$^{Akt\text{-}C}$, which resembles aggressive Richter transformation.[30] Integrative analysis of transcriptomes of cells from both models identified 8 B-cell clusters, of which 2 were predominantly enriched in *Eμ-TCL1A* mice (cluster 2 and 10), whereas 6 were enriched in *Eμ-TCL1A*$^{Akt\text{-}C}$ or shared with *Eμ-TCL1A* mice (cluster 0, 3, 13, 18, 19, and 20) (Figure 7G; supplemental Table 15). In *Eμ-TCL1A* mice, *Cdc20* expression was confined to the dominant cluster 2 (Figure 7H). In those *Eμ-TCL1A* B cells clustering with the more aggressive *Eμ-TCL1A*$^{Akt\text{-}C}$ B cells, hardly any *Cdc20* expression was detected. Differential gene expression analysis of the *Cdc20*-high vs all other clusters (*Cdc20*-low) identified 746 significant genes, of which most were upregulated in the *Cdc20*-high cluster. Consequently, most gene ontology processes were defined by genes upregulated in the *Cdc20*-high cluster (supplemental Figure 9B-D; supplemental Tables 16 and 17). In line with the patient data, *TCL1A* expression was higher in the *Cdc20*-negative clusters ($P < .001$; Figure 7I; supplemental Table 16). These data further confirm the more aggressive characteristics of cells with low *CDC20* expression.

CDC20 ablation accelerates leukemic outgrowth in mice

To validate the impact of modulated Cdc20 on murine CLL, we created from an *Eμ-TCL1A*–transplantable mouse model[51] a version with shRNA-mediated *Cdc20* knockdown (*Eμ-TCL1A;Cdc20-KD*; Figure 7J). At the early disease stage, a significantly faster outgrowth of Cd5$^+$/Cd19$^+$ B cells was observed in recipients transplanted with *Eμ-TCL1A;Cdc20-KD* cells (N = 15) as compared with mice transplanted with cells containing a GFP-coupled scramble shRNA vector (*Eμ-TCL1A;GFP*; N = 19; Figure 7K). The shorter survival of *Eμ-TCL1A;Cdc20-KD* mice was statistically not significant, likely owing to the highly aggressive character of the disease model (supplemental Figure 10A). Slightly elevated cyclin D1 levels ($P = .01$) and reduced PARP cleavage ($P = .048$) were seen in *Eμ-TCL1A;Cdc20-KD* mice, indicating higher proliferation rates and apoptotic resistance (Figure 7L; supplemental Figure 10B). This was paralleled by slightly elevated levels of pAkt and Bcl2 in *Eμ-TCL1A;Cdc20-KD* cells (supplemental Figure 10C). *Eμ-TCL1A;Cdc20-KD* tumors also acquired a significantly higher proportion of aneuploidy ($P = .014$) as compared with *Eμ-TCL1A;GFP* cells (Figure 7M).

Discussion

Although TCL1A is established to centrally contribute to T-cell and B-cell lymphomagenesis, the molecular concept of, particularly nuclear, TCL1A effectors and target pathways has remained incomplete. Most of the described TCL1A-interacting proteins can be assigned to the governance of cell survival.[13-15,52,53] Single-gene targeting of particular TCL1A executioners, that is, AKT1 or ATM, however, does not reproduce the phenotype of TCL1A-driven tumors.[17,54] Therefore, the spectrum of molecular and cell-biological consequences of TCL1A dysregulation, as well as the contexts (cell type, stimuli) in which such TCL1A-target engagements occur, are not fully represented by its recognized effectors.[18] Our animal experiments here implicate particularly nuclear TCL1A to be of highly transforming potential.

This study provides the first evidence for a modulating effect of TCL1A on mitotic progression and identifies a new and unique nuclear protein spectrum engaged by TCL1A. Through multiple proteomic analyses, we demonstrate that TCL1A interacts with

Figure 6. The interaction of TCL1A and CDC20 takes place via defined motifs and impairs CDC20's interaction with its negative regulators MAD2 and PLK1. (A) PLA of CLL-like MEC1 cells that were synchronized in mitosis (9 μM RO-3306 for 20 hours, 1 hour after release). TCL1A interacts with CDC20, MAD2, and CDK1 during mitosis. Quantification of PLA foci per cell is displayed in supplemental Figure 7A. (B) Images were taken using an SP8 confocal microscope (Leica) PLA for TCL1A and CDC20 was performed in MEC1 and HG3 CLL-like cells (synchronized as in panel A), and PLA foci per cell were quantified in mitotic and nonmitotic cells. Significantly more foci were counted in mitotic cells compared with nonmitotic cells. Negative control for MEC1: no primary antibody staining (Backgr.). Negative control for HG3: EV-transfected cells (TCL1A-negative HG3-EV) stained with primary antibodies. Boxes display medians with 25th to 75th percentiles and whiskers minimum and maximum; N = 25 cells (significances by one-way analysis of variance). Representative immunofluorescent images are in supplemental Figure 7C. (C) Split yellow fluorescent protein (YFP)–reporter principle of the protein complementation assay (PCA). Signal emission in living cells was induced upon noncovalent complementation of the N/C-terminal YFP components if the TCL1A-bait and the 'candidate' protein interact for >0.5 seconds. As a negative control, a construct encoding an ATG codon fused with the N-terminal part of YFP (ATG-YFP) was used to exclude fluorescence derived from spontaneous transient rejoining of split YFP parts. Images were taken on an Axio Scope.A1 microscope at original magnification ×100. (D) HeLa cells were cotransfected with TCL1A-YFP^N and CDC20-YFP^C constructs and the TCL1A-CDC20 interaction was visualized by the YFP signal (green). Cytoskeleton and DNA were visualized by rhodamine-phalloidin (red) and Hoechst (blue), respectively. Prominent signals corresponding to the specific TCL1A-CDC20 interaction accumulated at the mitotic plate and dispersed during anaphase. (E) Five constructs of indicated CDC20 variants were generated by PCR-mediated site-directed mutagenesis (top) and were used in co-IPs in HEK293 cells to interrogate sequence restrictions of the CDC20-TCL1A interaction (bottom). RCRY^{4A} and del(97-169) nearly completely abolished the interaction. (F) The CDC20-TCL1A complex was predicted based on the published experimental protein structures of CDC20 (pdb ID 4GGA) and TCL1A (pdb ID 1JSG). Predictive tools to propose putative interfaces (CPORT)[36] were used and the outputs exploited in the High Ambiguity Driven protein-protein DOCKing 2.2 (HADDOCK 2.2) algorithm for modeling biomolecular complexes.[37] This in silico modeling predicted 2 potential models, which differ in the amino acids (aa) of TCL1A involved in this interaction. The residues E40, K42, and Y96 of TCL1A are expected to stabilize the TCL1A-CDC20 interaction in model A, whereas E9, R93, and Y96 would promote this interaction in model B. Detailed HADDOCK statistics are summarized in supplemental Tables 12 and 13. (G) TCL1A mutants used in co-IP studies (top). They represent model A (EKY^{SAE}, in red) with the aa substitutions E40S, K42A, and Y96E, and model B (ERY^{KDE}, blue) with E9K, R93D, and Y96E. CDC20 co-IP of lysates from JVM3 cells stably overexpressing TCL1A-FLAG, TCL1A-EKY^{SAE}-FLAG, or TCL1A-ERY^{KDE}-FLAG (bottom). Cells were synchronized before in G2 by 9 μM RO-3306 for 20 hours. In the last 5 hours, 10 μM MG132 was added to reduce protein degradation of the 2 mutants. The EKY^{SAE} (model A) nearly abolished the TCL1A-CDC20 interaction. (H) PLA for CDC20 and MAD2 was performed in MEC1-shTCL1A (TCL1A knockdown) vs -shCtrl cells as well as in HG3-EV vs -TCL1A (TCL1A introduction) cells. Significantly less PLA foci were counted per cell in the TCL1A-expressing/-high lines, suggesting an impaired CDC20-MAD2 interaction in the presence of TCL1A. Boxes display medians with 25th to 75th percentiles and whiskers minimum and maximum; N = 40 cells (significances as per Student *t* test). Images were taken using an SP8 confocal microscope. (I) JVM3 ± TCL1A cells were synchronized in G2 by 9 μM RO-3306 for 20 hours and released in full medium. CDC20-IP was performed in lysates at indicated time points to determine CDC20-PLK1 interaction. IgG control: pooled lysates of JVM3^{EV} and JVM3^{TCL1A}. CMV, cytomegalovirus; DAPI, 4′,6-diamidino-2-phenylindole; MIM, MAD2-interacting motif; neg, negative.

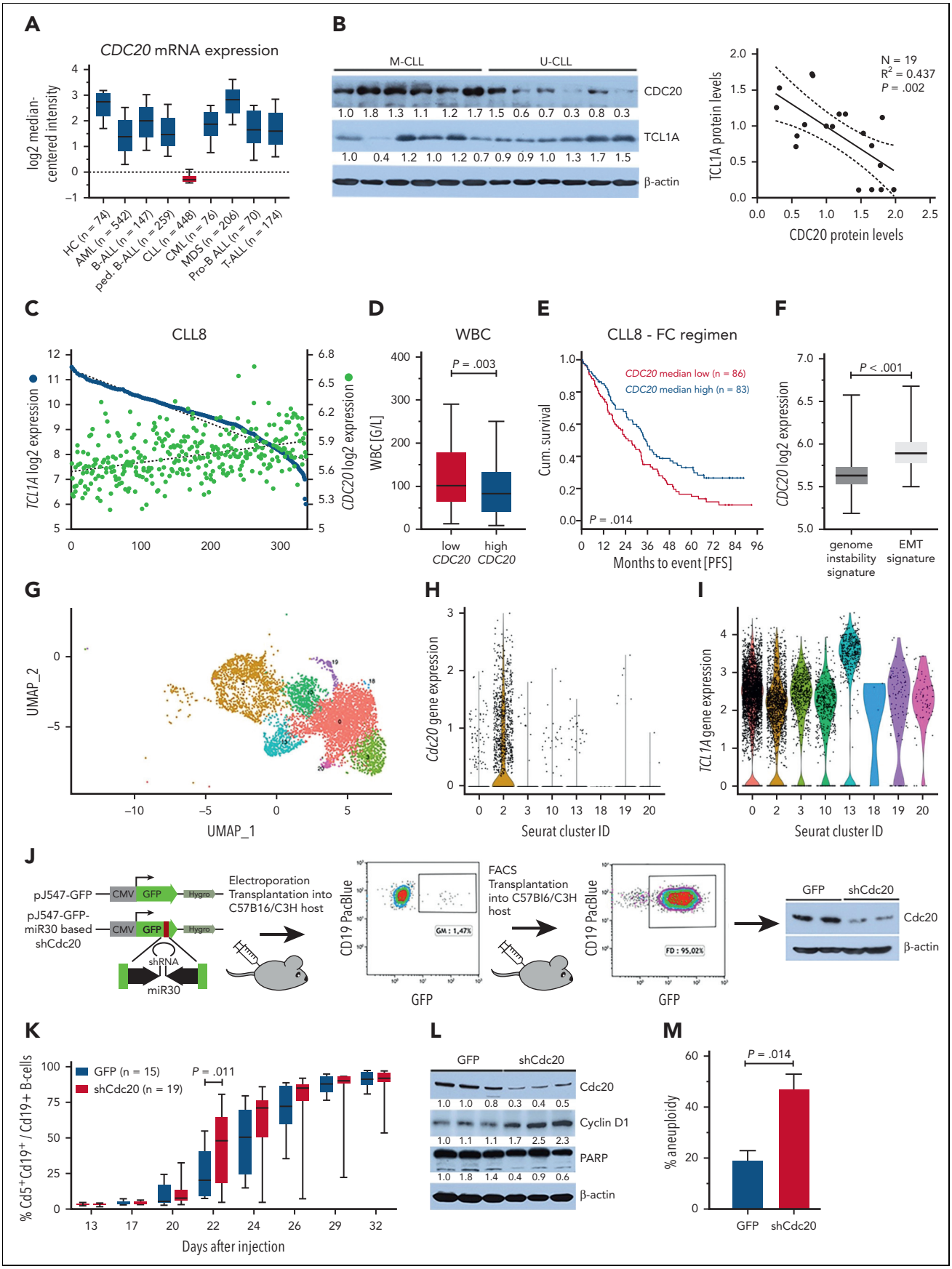

Figure 7.

a range of proteins that orchestrate DDR pathways, particularly cell cycle checkpoints. The cell cycle was one of the most prominent functional clusters enriched in the TCL1A interactome and its key regulatory molecules such as, CDC20, CDK1, or MAD2, colocalized with TCL1A in the cytoplasm and at the mitotic spindle.

The observed cellular consequences of (enforced) TCL1A expression in several CLL-like cell lines[55] and in *Eμ-TCL1A* mice, that is, an accelerated entry and transition through mitosis, corroborate these molecular findings. Further in line with this new mode of TCL1A's action, a higher rate of aneuploidy coincided with a higher incidence of multipolar spindles and aberrant responses to DNA damage. The primary occurrence of aneuploidy in preleukemic *Eμ-TCL1A* mice indicates a direct TCL1A effect rather than this being a secondary phenomenon of tumor progression.

At the core of our findings, we established a direct physical interaction of TCL1A with the APC/C cofactor CDC20. In contrast to its interaction with AKT,[42] a disrupted dimerization of TCL1A did not influence TCL1A-CDC20 complex formation, suggesting that TCL1A interacts with CDC20 before its homodimerization, or that interaction of CDC20 with monomeric TCL1A is functionally sufficient. Through a combined biochemical and in silico–modeling approach, we defined the crucial regions of the TCL1A-CDC20 interaction with the aa E40, K42, and Y96 of TCL1A as well as the MIM- and CRY-boxes of CDC20, which are important degrons in regulating the MCC to APC/C switch.[23,56] Therefore, our structure-based predictions suggest a functional consequence of TCL1A-bound CDC20 on the MCC and/or APC/C. Indeed, we identified a TCL1A-associated disrupted interaction of CDC20 with its negative regulators, MAD2 (sequestration of CDC20 by the MCC[23]) and PLK1 (inhibitory phosphorylation).[45] These data imply TCL1A to perturb proper mitotic checkpoint function, likely contributing to accelerated cell cycle transition and accumulating aneuploidy.

Is potentially tumor-suppressing CDC20 relevant in CLL? We observed a strong CLL-specific transcriptional *CDC20* downregulation, which correlated inversely with *TCL1A* expression. Lower expression of *CDC20* in CLL was associated with higher genomic instability. Patients with *CDC20*-low CLL had a shorter PFS after chemotherapy. Lower *CDC20* is likely part of the transcriptional programs of the more aggressive TCL1A-high subset of U-CLL. Nevertheless, we demonstrated a rather direct causal proleukemic impact of reduced CDC20 in the context of TCL1A overexpression by experimental *Cdc20* downmodulation, which accelerated leukemic progression and higher rates of aneuploidy in the *Eμ-TCL1A* CLL model. At the single-cell level of TCL1A-induced murine CLL, *Cdc20*-low/negative clusters showed the highest *TCL1A* expression and were associated with a more aggressive phenotype, for example, in our model of Richter transformation. Interestingly and in contrast to our observations in CLL, higher levels of CDC20 in solid tumors (normally TCL1A-negative) are associated with treatment resistance, dissemination, and poor prognosis.[57-59] Such a particular dual relationship of a TCL1A target protein and a downregulated safeguarding molecule is already shown for the TCL1A-ATM interaction.[2,4,52]

Overall, our findings add valuable new insights to the molecular concept of, thus far underappreciated nuclear, executioners of oncogenic TCL1A. We conclude that TCL1A overexpression promotes premature, DNA damage–prone cell cycle checkpoint transition, which in context-specific synergy with impaired damage repair and hyperactive prosurvival signaling (see the visual abstract on the *Blood* website) mediates the transforming impact of TCL1A. This provides a rationale for more informed targeting strategies.

Acknowledgments

The authors thank S. Michnick (University of Montreal, Canada) for the provision of constructs. Chronic lymphocytic leukemia (CLL) sample acquisition was supported by the Biobank of the Center for Integrated Oncology Aachen Bonn Cologne Düsseldorf (CIO ABCD) funded by the German Cancer Aid. The analysis of gene expression profile data of the

Figure 7. CDC20 expression is reduced in CLL and correlates with a more aggressive cell and disease phenotype. (A) *CDC20* expression in different lymphatic and myeloid neoplasms as measured by microarray-based gene expression profiling (data set of Haferlach et al).[50] Boxes with medians and 25th to 75th percentiles. Whiskers show 10th and 90th percentiles. CLL stands out among the other hematopoietic cancers, as its *CDC20* expression is markedly reduced; for example, FCh = −6.8; $P < .001$ compared with healthy controls. (B) Expression of TCL1A and CDC20 in primary human CLL cells. Representative immunoblot showing decreased CDC20 expression in lysates from unstimulated U-CLL (N = 6) vs M-CLL (N = 6) (left). Linear regression analysis demonstrates an inverse correlation of TCL1A and CDC20 protein levels in CLL (N = 19; $P = .002$; $R = 0.437$) (right). (C) GEP of previously untreated patients with CLL (N = 337) of the prospective CLL8 trial identified an inverse correlation of *TCL1A* (blue) and *CDC20* (green) expression. (D) Patients from the CLL8 trial were divided into 2 groups by the median expression of *CDC20*. Patients with low *CDC20* expression (N = 166, red) showed significantly higher WBC counts in comparison with those with high *CDC20* (N = 163, blue). Boxes show medians and the 25th to 75th percentiles, whiskers the 10th to 90th percentiles. Significance was determined using the median test. (E) Patients from the CLL8 trial that received fludarabine/cyclophosphamide (FC) were divided into 2 groups by the median expression of *CDC20*. The Kaplan-Meier curve illustrates the significantly shorter progression-free survival (PFS) of patients with low *CDC20* expression (N = 86; green; median PFS, 25.5 months) compared with those with high *CDC20* expression (N = 83; blue; median PFS, 34.1 months); $P = .014$, log-rank test. (F) *CDC20* expression levels are significantly lower in CLL that we previously characterized by a molecular profile of genome instability (N = 189)[29] than in those with activation of epithelial-mesenchymal transition (EMT)–like programs (N = 130; $P < .001$, Mann-Whitney test). Boxes with medians, 25th to 75th percentiles, and whiskers of mininum/maximum. (G) Reanalysis of single-cell RNA sequencing data from *Eμ-TCL1A* and *Eμ-TCL1A*$^{Akt\text{-}C}$ (Richter syndrome model) mice that we published in Kohlhaas et al.[30] The UMAP displays the clusters identified in the integrative analysis of both models that were then applied to the *Eμ-TCL1A* model only (N = 4 mice). Clusters 2 and 10 are enriched in *Eμ-TCL1A* cells, whereas clusters 0, 3, 13, 18, 19, and 20 represent *Eμ-TCL1A*$^{Akt\text{-}C}$ or those that are shared with *Eμ-TCL1A*. (H) *Cdc20* is primarily expressed in the *Eμ-TCL1A* enriched Seurat cluster 2. (I) *TCL1A* expression is significantly lower in Seurat cluster 2 compared with all other clusters, $P < .001$ (supplemental Table 16). (J) Setup of in vivo *Cdc20* knockdown experiment: leukemic *Eμ-TCL1A* splenocytes[51] were nucleofected with the transposon-based pJ547-shCdc20 construct. It encodes a GFP cassette with microRNA 30 (miR-30)–based shRNA sequences against murine Cdc20 at the 3′ end. A pJ547-GFP control encoded an unspecific shRNA sequence. After intraperitoneal injection into syngeneic hosts and tumor development, GFP$^+$ splenocytes were purified using fluorescence-activated cell sorter (FACS) and reinjected into hosts. Knockdown efficiency was tested by immunoblots (right). (K) Flow-cytometric analysis of PB cells showing a faster increase of the aberrant leukemic Cd5$^+$ Cd19$^+$ B-cell population in recipients that were transplanted with *Eμ-TCL1A;Cdc20-KD* B cells (N = 19) compared with *Eμ-TCL1A;*GFP control animals (N = 15). Boxes indicate medians and 25th to 75th percentiles and whiskers show minimum and maximum; significance was tested using a two-way analysis of variance with Bonferroni correction for multiple testing. (L) Immunoblot analysis showing increased cyclin D1 and slightly reduced PARP cleavage in splenocytes from *Eμ-TCL1A;Cdc20-KD* compared with *Eμ-TCL1A;GFP* mice. Splenocytes were isolated at the end point of survival analysis. Each lane represents an individual animal. (M) The proportion of metaphases with an aberrant number of chromosomes was significantly higher in *Eμ-TCL1A;Cdc20-KD* cells compared with *Eμ-TCL1A;GFP* cells (Student *t* test). AML, acute myeloid leukemia; B-ALL, B-cell acute lymphoblastic leukemia; CML, chronic myeloid leukemia; hygro, hygromycin resistance; MDS, myelodysplastic syndrome; ped., pediatric.

CLL8 trial was supported by the German CLL Study Group. Mass spectrometry analyses were conducted at the Cologne Excellence Cluster on Stress Responses in Aging-Associated Diseases proteomics facility. Use of Olympus microscopes was provided by the microscopy core facility of the Center for Molecular Medicine Cologne (CMMC, Germany). Sample processing and single-cell RNA sequencing was performed by M. Franitza, J. Altmüller, and T. Georgomanolis (Cologne Center for Genomics). Preprocessing of single-cell RNA sequencing data was performed by M. Nikolic and M. Peifer (CMMC).

This work was supported by grants from the German Research Foundation (DFG, HE-3553/3-2) (M. Herling [PI] and E.V. [female research grant]) as part of the collaborative research group KFO-286 and from the CMMC Program (Project C08; Project 23-RP) (M. Herling and E.V.). M. Herling was funded by the José Carreras Leukemia Foundation (R12/08) and the DFG Research Unit FOR1961 (Control-T; HE3553/4-2). E.V. received financial support from Köln Fortune Program (110/2012), German Cancer Aid (70112788), Nolting, Kaethe-Hack, and Hochhaus Foundations.

Authorship

Contribution: E.V., J.S., Q.J., C.A., M. Hallek, S.S., J.B., and M. Herling designed the experiments and analyzed the in vitro–generated data; E.V., J.S., C.A., Q.J., T.M., O.V., K.S., and P.M. performed the in vitro experiments; E.V., K.W., G.C., and S.N. designed, performed, and analyzed the in vivo experiments and gene expression profile data of mice; M.K., J.S., and C.A. performed mass spectrometry experiments and statistical analyses; G.G., S. Hippler, and K.-A.K. performed cytogenetic analyses; A.L. and D.B. acquired human tissue samples; N.B. and S. Hüttelmaier performed proximity ligation assay experiments; J.B., S.R., K.F., and S.S. acquired and analyzed gene expression profiles and clinical data of the CLL8 trial; S.J.B. and C.P. performed single-cell RNA sequencing data analysis; D.A. performed the molecular modelling and the in silico analysis of protein complexes; and E.V., J.S., and M. Herling wrote the manuscript.

Conflict-of-interest disclosure: The authors declare no competing financial interests.

Elena Vasyutina died on 24 February 2020.

ORCID profiles: J.S., 0000-0001-7419-8900; N.B., 0000-0002-4531-7998; C.P., 0000-0001-5675-6905; M.K., 0000-0002-5846-6941; D.A., 0000-0003-4713-9096; J.B., 0000-0003-1433-9702.

Correspondence: Marco Herling, Department of Hematology, Cellular Therapy, and Hemostaseology, University of Leipzig Medical Center, Liebigstr. 22, 04103 Leipzig, Germany; email: marco.herling@medizin.uni-leipzig.de.

Footnotes

Submitted 12 January 2022; accepted 4 September 2022; prepublished online on *Blood* First Edition 20 September 2022. https://doi.org/10.1182/blood.2022015494.

*J.B., E.V., and M.H. contributed equally to this study.

Microarray data reported in this article have been deposited in the Gene Expression Omnibus database (accession numbers GSE126595 [CLL8][29] and GSE192409 [murine gene expression profile data]). The mass spectrometry–based proteomics data have been deposited at the ProteomeXchange Consortium via the PRIDE[31] partner repository (data set identifiers PXD029961, PXD030776, and PXD030773).

Data are available on request from the corresponding author, Marco Herling (marco.herling@medizin.uni-leipzig.de).

The online version of this article contains a data supplement.

There is a *Blood* Commentary on this article in this issue.

The publication costs of this article were defrayed in part by page charge payment. Therefore, and solely to indicate this fact, this article is hereby marked "advertisement" in accordance with 18 USC section 1734.

REFERENCES

1. Virgilio L, Narducci MG, Isobe M, et al. Identification of the TCL1 gene involved in T-cell malignancies. *Proc Natl Acad Sci U S A*. 1994;91(26):12530-12534.
2. Schrader A, Crispatzu G, Oberbeck S, et al. Actionable perturbations of damage responses by TCL1/ATM and epigenetic lesions form the basis of T-PLL. *Nat Commun*. 2018;9(1):697.
3. Pekarsky Y, Zanesi N, Croce CM. Molecular basis of CLL. *Semin Cancer Biol*. 2010;20(6):370-376.
4. Herling M, Patel KA, Khalili J, et al. TCL1 shows a regulated expression pattern in chronic lymphocytic leukemia that correlates with molecular subtypes and proliferative state. *Leukemia*. 2006;20(2):280-285.
5. Herling M, Patel KA, Teitell MA, et al. High TCL1 expression and intact T-cell receptor signaling define a hyperproliferative subset of T-cell prolymphocytic leukemia. *Blood*. 2008;111(1):328-337.
6. Herling M, Patel KA, Weit N, et al. High TCL1 levels are a marker of B-cell receptor pathway responsiveness and adverse outcome in chronic lymphocytic leukemia. *Blood*. 2009;114(21):4675-4686.
7. Hopfinger G, Busch R, Pflug N, et al. Sequential chemoimmunotherapy of fludarabine, mitoxantrone, and cyclophosphamide induction followed by alemtuzumab consolidation is effective in T-cell prolymphocytic leukemia. *Cancer*. 2013;119(12):2258-2267.
8. Ramuz O, Bouabdallah R, Devilard E, et al. Identification of TCL1A as an immunohistochemical marker of adverse outcome in diffuse large B-cell lymphomas. *Int J Oncol*. 2005;26(1):151-157.
9. Herling M, Patel KA, Hsi ED, et al. TCL1 in B-cell tumors retains its normal b-cell pattern of regulation and is a marker of differentiation stage. *Am J Surg Pathol*. 2007;31(7):1123-1129.
10. Aggarwal M, Villuendas R, Gomez G, et al. TCL1A expression delineates biological and clinical variability in B-cell lymphoma. *Mod Pathol*. 2009;22(2):206-215.
11. Virgilio L, Lazzeri C, Bichi R, et al. Deregulated expression of TCL1 causes T cell leukemia in mice. *Proc Natl Acad Sci U S A*. 1998;95(7):3885-3889.
12. Bichi R, Shinton SA, Martin ES, et al. Human chronic lymphocytic leukemia modeled in mouse by targeted TCL1 expression. *Proc Natl Acad Sci U S A*. 2002;99(10):6955-6960.
13. Pekarsky Y, Koval A, Hallas C, et al. Tcl1 enhances Akt kinase activity and mediates its nuclear translocation. *Proc Natl Acad Sci U S A*. 2000;97(7):3028-3033.
14. Laine J, Künstle G, Obata T, Sha M, Noguchi M. The protooncogene TCL1 is an Akt kinase coactivator. *Mol Cell*. 2000;6(2):395-407.
15. Pekarsky Y, Palamarchuk A, Maximov V, et al. Tcl1 functions as a transcriptional regulator and is directly involved in the pathogenesis of CLL. *Proc Natl Acad Sci U S A*. 2008;105(50):19643-19648.
16. Oberbeck S, Schrader A, Warner K, et al. Noncanonical effector functions of the T-memory-like T-PLL cell are shaped by cooperative TCL1A and TCR signaling. *Blood*. 2020;136(24):2786-2802.
17. Kharas MG, Okabe R, Ganis JJ, et al. Constitutively active AKT depletes hematopoietic stem cells and induces leukemia in mice. *Blood*. 2010;115(7):1406-1415.
18. Stachelscheid J, Jiang Q, Herling M. The modes of dysregulation of the proto-oncogene T-cell leukemia/lymphoma 1A. *Cancers (Basel)*. 2021;13(21):5455.
19. Klein U, Lia M, Crespo M, et al. The DLEU2/miR-15a/16-1 cluster controls B cell proliferation and its deletion leads to chronic lymphocytic leukemia. *Cancer Cell*. 2010;17(1):28-40.
20. Kienle DL, Korz C, Hosch B, et al. Evidence for distinct pathomechanisms in genetic subgroups of chronic lymphocytic leukemia revealed by quantitative expression

analysis of cell cycle, activation, and apoptosis-associated genes. *J Clin Oncol*. 2005;23(16):3780-3792.

21. Decker T, Schneller F, Hipp S, et al. Cell cycle progression of chronic lymphocytic leukemia cells is controlled by cyclin D2, cyclin D3, cyclin-dependent kinase (cdk) 4 and the cdk inhibitor p27. *Leukemia*. 2002;16(3):327-334.
22. Schmidt M, Rohe A, Platzer C, et al. Regulation of G2/M transition by inhibition of WEE1 and PKMYT1 kinases. *Molecules*. 2017; 22(12):2045.
23. Chao WCH, Kulkarni K, Zhang Z, Kong EH, Barford D. Structure of the mitotic checkpoint complex. *Nature*. 2012;484(7393):208-213.
24. Vleugel M, Hoogendoorn E, Snel B, Kops GJPL. Evolution and function of the mitotic checkpoint. *Dev Cell*. 2012;23(2):239-250.
25. Fedorchenko O, Stiefelhagen M, Peer-Zada AA, et al. CD44 regulates the apoptotic response and promotes disease development in chronic lymphocytic leukemia. *Blood*. 2013;121(20):4126-4136.
26. Newrzela S, Cornils K, Li Z, et al. Resistance of mature T cells to oncogene transformation. *Blood*. 2008;112(6):2278-2286.
27. Hallek M, Fischer K, Fingerle-Rowson G, et al. Addition of rituximab to fludarabine and cyclophosphamide in patients with chronic lymphocytic leukaemia: a randomised, open-label, phase 3 trial. *Lancet*. 2010;376(9747): 1164-1174.
28. Vasyutina E, Boucas JM, Bloehdorn J, et al. The regulatory interaction of EVI1 with the TCL1A oncogene impacts cell survival and clinical outcome in CLL. *Leukemia*. 2015; 29(10):2003-2014.
29. Bloehdorn J, Braun A, Taylor-Weiner A, et al. Multi-platform profiling characterizes molecular subgroups and resistance networks in chronic lymphocytic leukemia. *Nat Commun*. 2021;12(1):5395.
30. Kohlhaas V, Blakemore SJ, Al-Maarri M, et al. Active Akt signaling triggers CLL toward Richter transformation via overactivation of Notch1. *Blood*. 2021;137(5):646-660.
31. Perez-Riverol Y, Csordas A, Bai J, et al. The PRIDE database and related tools and resources in 2019: improving support for quantification data. *Nucleic Acids Res*. 2019; 47(D1):D442-D450.
32. Sancar A, Lindsey-Boltz LA, Unsal-Kaçmaz K, Linn S. Molecular mechanisms of mammalian DNA repair and the DNA damage checkpoints. *Annu Rev Biochem*. 2004;73(1): 39-85.
33. Bailis JM, Forsburg SL. MCM proteins: DNA damage, mutagenesis and repair. *Curr Opin Genet Dev*. 2004;14(1):17-21.
34. Kaneta Y, Ullrich A. NEK9 depletion induces catastrophic mitosis by impairment of mitotic checkpoint control and spindle dynamics. *Biochem Biophys Res Commun*. 2013; 442(3-4):139-146.
35. Lara-Gonzalez P, Moyle MW, Budrewicz J, et al. The G2-to-M transition is ensured by a dual mechanism that protects cyclin B from degradation by Cdc20-activated APC/C. *Dev Cell*. 2019;51(3):313-325.e10.
36. de Vries SJ, Bonvin AMJJ. CPORT: a consensus interface predictor and its performance in prediction-driven docking with HADDOCK. *PLoS One*. 2011;6(3): e17695.
37. Dominguez C, Boelens R, Bonvin AMJJ. HADDOCK: a protein-protein docking approach based on biochemical or biophysical information. *J Am Chem Soc*. 2003;125(7):1731-1737.
38. Michnick SW, Ear PH, Landry C, Malleshaiah MK, Messier V. Protein-fragment complementation assays for large-scale analysis, functional dissection and dynamic studies of protein-protein interactions in living cells. *Methods Mol Biol*. 2011;756: 395-425.
39. Pfleger CM, Lee E, Kirschner MW. Substrate recognition by the Cdc20 and Cdh1 components of the anaphase-promoting complex. *Genes Dev*. 2001;15(18): 2396-2407.
40. Labit H, Fujimitsu K, Bayin NS, et al. Dephosphorylation of Cdc20 is required for its C-box-dependent activation of the APC/C. *EMBO J*. 2012;31(15):3351-3362.
41. Ge S, Skaar JR, Pagano M. APC/C- and Mad2-mediated degradation of Cdc20 during spindle checkpoint activation. *Cell Cycle*. 2009;8(1):167-171.
42. Auguin D, Barthe P, Royer C, et al. Structural basis for the co-activation of protein kinase B by T-cell leukemia-1 (TCL1) family proto-oncoproteins. *J Biol Chem*. 2004;279(34): 35890-35902.
43. Dosztányi Z, Csizmok V, Tompa P, Simon I. IUPred: web server for the prediction of intrinsically unstructured regions of proteins based on estimated energy content. *Bioinformatics*. 2005;21(16): 3433-3434.
44. Izawa D, Pines J. Mad2 and the APC/C compete for the same site on Cdc20 to ensure proper chromosome segregation. *J Cell Biol*. 2012;199(1):27-37.
45. Jia L, Li B, Yu H. The Bub1–Plk1 kinase complex promotes spindle checkpoint signalling through Cdc20 phosphorylation. *Nat Commun*. 2016;7(1):10818.
46. Landau DA, Carter SL, Stojanov P, et al. Evolution and impact of subclonal mutations in chronic lymphocytic leukemia. *Cell*. 2013; 152(4):714-726.
47. Landau DA, Tausch E, Taylor-Weiner AN, et al. Mutations driving CLL and their evolution in progression and relapse. *Nature*. 2015;526(7574):525-530.
48. Quesada V, Conde L, Villamor N, et al. Exome sequencing identifies recurrent mutations of the splicing factor SF3B1 gene in chronic lymphocytic leukemia. *Nat Genet*. 2011;44(1):47-52.
49. Puente XS, Beà S, Valdés-Mas R, et al. Non-coding recurrent mutations in chronic lymphocytic leukaemia. *Nature*. 2015; 526(7574):519-524.
50. Haferlach T, Kohlmann A, Wieczorek L, et al. Clinical utility of microarray-based gene expression profiling in the diagnosis and subclassification of leukemia: report from the International Microarray Innovations in Leukemia Study Group. *J Clin Oncol*. 2010; 28(15):2529-2537.
51. Suljagic M, Longo PG, Bennardo S, et al. The Syk inhibitor fostamatinib disodium (R788) inhibits tumor growth in the Eμ- TCL1 transgenic mouse model of CLL by blocking antigen-dependent B-cell receptor signaling. *Blood*. 2010;116(23):4894-4905.
52. Gaudio E, Spizzo R, Paduano F, et al. Tcl1 interacts with Atm and enhances NF-κB activation in hematologic malignancies. *Blood*. 2012;119(1):180-187.
53. Sivina M, Hartmann E, Vasyutina E, et al. Stromal cells modulate TCL1 expression, interacting AP-1 components and TCL1-targeting micro-RNAs in chronic lymphocytic leukemia. *Leukemia*. 2012;26(8):1812-1820.
54. Barlow C, Hirotsune S, Paylor R, et al. Atm-deficient mice: a paradigm of ataxia telangiectasia. *Cell*. 1996;86(1):159-171.
55. Lanemo Myhrinder A, Hellqvist E, Bergh A-C, et al. Molecular characterization of neoplastic and normal "sister" lymphoblastoid B-cell lines from chronic lymphocytic leukemia. *Leuk Lymphoma*. 2013;54(8):1769-1779.
56. Yamaguchi M, VanderLinden R, Weissmann F, et al. Cryo-EM of mitotic checkpoint complex-bound APC/C reveals reciprocal and conformational regulation of ubiquitin ligation. *Mol Cell*. 2016;63(4): 593-607.
57. Wang S, Chen B, Zhu Z, et al. CDC20 overexpression leads to poor prognosis in solid tumors: a system review and meta-analysis. *Medicine (Baltimore)*. 2018;97(52): e13832.
58. Alfarsi LH, Ansari R El, Craze ML, et al. CDC20 expression in oestrogen receptor positive breast cancer predicts poor prognosis and lack of response to endocrine therapy. *Breast Cancer Res Treat*. 2019;178(3):535-544.
59. Song C, Lowe VJ, Lee S. Inhibition of Cdc20 suppresses the metastasis in triple negative breast cancer (TNBC). *Breast Cancer*. 2021; 28(5):1073-1086.